

The Bolund Experiment: Overview and Background

Risø-R-Report

Andreas Bechmann, Jacob Berg, Michael S. Courtney, Hans E. Jørgensen, Jakob Mann and Niels N. Sørensen
Risø-R-1658(EN)
July 2009



Author: Andreas Bechmann¹, Jacob Berg², Michael S. Courtney³, Hans E. Jørgensen², Jakob Mann² and Niels N. Sørensen¹
Title: The Bolund Experiment: Overview and Background
Division: 1 Aeroelastic Design – Wind Energy Division
2 Meteorology – Wind Energy Division
3 Test and Measurements – Wind Energy Division

Abstract (max. 2000 char.):

The Bolund experiment is a measuring campaign performed in 2007 and 2008. The aim of the experiment is to measure the flow field around the Bolund hill in order to provide a dataset for validating numerical flow models. The present report gives an overview of the whole experiment including a description of the orography, the instrumentation used and of the data processing. The Actual measurements are available from a database also described.

Risø-R-1658(EN)
July 2009

ISSN 0106-2840
ISBN 978-87-550-3703-8

Contract no.:
ENS-33033-0062

Group's own reg. no.:
1110058-01

Sponsorship:
Energistyrelsen,
Danish Energy Agency,
Vestas Technology R&D

Cover :
Picture of the Bolund hill

Pages: 51
Tables: 20
References: 13

Information Service Department
Risø National Laboratory for
Sustainable Energy
Technical University of Denmark
P.O.Box 49
DK-4000 Roskilde
Denmark
Telephone +45 46774005
bibl@risoe.dtu.dk
Fax +45 46774013
www.risoe.dtu.dk

Contents

1	Preface	<i>5</i>
2	Summary	<i>6</i>
2.1	Background	<i>6</i>
2.2	Overview of the Bolund Experiment	<i>7</i>
3	Site Details	<i>9</i>
3.1	General Site Description	<i>9</i>
3.2	Scale Effects	<i>12</i>
3.3	Contour Map	<i>13</i>
4	Experimental Setup	<i>17</i>
4.1	Overview	<i>17</i>
4.2	Water Level	<i>18</i>
4.3	Data Acquisition	<i>18</i>
4.4	Sonic Anemometers	<i>19</i>
4.5	Cup Anemometers	<i>20</i>
4.6	Temperature	<i>20</i>
4.7	Lidar	<i>21</i>
4.8	Measuring Positions and Instrumentation ID	<i>22</i>
5	Sonic Data Processing	<i>29</i>
5.1	Metek3d Corrections	<i>29</i>
5.2	Velocity corrections	<i>30</i>
5.3	Temperature corrections	<i>31</i>
5.4	Statistics	<i>32</i>
6	MySQL database	<i>39</i>
6.1	Overview	<i>39</i>
6.2	Tables in MySql	<i>39</i>
6.3	Example 1: Retrieving sonic data	<i>40</i>
6.4	Example 2: Retrieving cup data	<i>41</i>
6.5	Example 3: Retrieving lidar data	<i>42</i>

Appendix A: Optech Airborne Laser Terrain Mapper, ALTM 3100EA 43

Appendix B: Diagram of instrumentation 45

Appendix C: 3D Correction Look-up Tables 47

References 49

1 Preface

The Bolund experiment is a field campaign that provides a unique dataset for validating models designed for flow in complex terrain. The experiment was conducted from December 2007 to February 2008 on the Bolund hill located 1 km north of Risø DTU, National Laboratory for Sustainable Energy. The present report describes the background of the Bolund Experiment and gives a detailed description of the measurement campaign.

The work is conducted within the EFP project:

EFP07 - Metoder til kortlægning af vindforhold i komplekst terræn. (ENS-33033-0062)

Risø DTU has conducted the measurement campaign in corporation with Vestas Technology R&D who has provided part of the funding for the project.

2 Summary

This report contains background information of the Bolund experiment. The Bolund experiment is a measurement campaign performed in 2007 and 2008. The Bolund hill is a 12 m high peninsula located at Roskilde Fjord 1 km north of Risø DTU near the city of Roskilde (Denmark). Bolund was selected for a field experiment because of the need for experimental data for validating models of flow in complex terrain. An increasing number of wind farms are being installed in complex terrain, but the tools often used to predict the wind flow have been developed for simple terrain and have not been properly validated against complex terrain experiments at atmospheric scale. The Bolund dataset allows for such a validation. Though relatively small, Bolund has a geometrical shape that characterizes many complex sites e.g. a well-exposed, almost vertical upstream escarpment and an isolated location with well-defined inflow from the sea.

The present report describes the actual experiment that was conducted from December 2007 to February 2008. The report describes the Bolund orography and wind climate as well as the instrumentation and data processing used for the experiment. The actual measurements are available through a database, which is also described in this report. A description of how the experiment was designed using CFD can be found in [1].

2.1 Background

Today, a large number of wind farms are erected in complex terrain with the hope of a large energy production. By placing wind turbines in hilly terrain, along ridges and even in mountainous areas, wind phenomena like flow separation and recirculation can, however, greatly increase the structural loads on the wind turbines. Reliable predictions of such wind features are therefore important for siting of wind turbines in complex terrain and is the subject of the Bolund experiment.

Many of the current commercial flow solvers are based on linearization of the Navier-Stokes equations. In order for such solvers to perform accurately, limits on the complexity of the terrain must be kept i.e. the slopes of the terrain and the changes in roughness must be small. Since wind turbines are placed in complex terrain that induce non-linear flow, there is a demand from the wind energy community for continuous development and validation of non-linear models.

Numerous numerical models for the calculation of flow and turbulence over complex terrain exist; from the linearized Jackson-Hunt type models [2] to many sophisticated non-linear models: RANS, DES, LES, etc. Common for all these are that they use the famous Askervein experiment for validation [3, 4]. This experiment took place 25 years ago but despite limited instruments and data acquisition capabilities, both mean velocity and turbulence data were recorded. The Askervein hill shape was nearly Gaussian with not too steep slopes and was primarily selected as a validation case for linear analysis and linearized models in both 2D and 3D. Today, the Askervein hill is not sufficiently challenging for the numerical codes and there is a demand for new experimental data in complex terrain. The Bolund experiment provides just such a dataset.

The ambitious objective of the Bolund experiment is to increase our understanding of boundary layer flow in complex terrain and to provide a new dataset for development of computational flow solvers, especially in relation to siting of wind turbines. Detailed measurements of mean wind ('speed-up', inclination, shear) and turbulence (variance, stress, autocorrelation) over a very steep terrain will be provided to the community, to be compared with any flow model for complex terrain that is available.



Figure 1. Picture of Bolund from the 125 m high measuring mast at Risø DTU.

2.2 Overview of the Bolund Experiment

Bolund is a 12 m high, 130 m long and a 75 m wide coastal hill located just north of Risø DTU (see Figure 1). The geometrical shape of the hill consists of properties that characterize a complex terrain. Properties like a well-exposed almost vertical upstream escarpment, a sharp change in surface roughness with the wind passing from water to grass and a highly complex three-dimensional geometry make the Bolund hill a challenging test case for any numerical flow solver. A detailed description of the Bolund orography is found in Section 3.1.

The Bolund hill is too small to represent a wind turbine site. However, the relative low height of Bolund can actually be seen as a benefit when validating numerical codes. Because of the low height, thermal and Coriolis effects can mostly be neglected, and a more well-defined code validation is possible. Scale effects are further discussed in Section 3.2.

The predominant wind direction during the experiment was south southwest (see Figure 2). With winds from west there is a long fetch of sea of approximately 7 km (270°), while the fetch with the wind from west southwest (239°) is about 4 km. On figure 2 the turbulence intensity at 12 m height 100 m west of Bolund is shown (axis markings has deliberately been removed). Here it is seen that the turbulence intensity increases when the wind changes from west to south, indicating the clear fetch for westerly winds. Since the inflow conditions are well defined from the (270°) and (239°) directions, lines along these directions through the hill centerpoint (CP) have been chosen as regions of main interest (line A and B in Figure 3). Having a long upstream fetch ensures that the incoming wind is in a state of equilibrium and is horizontally homogeneous. This is important, since the "undisturbed" wind conditions are necessary when using the experiment as a validation case for numerical codes. A description of the experimental setup is found in Chapter 4.

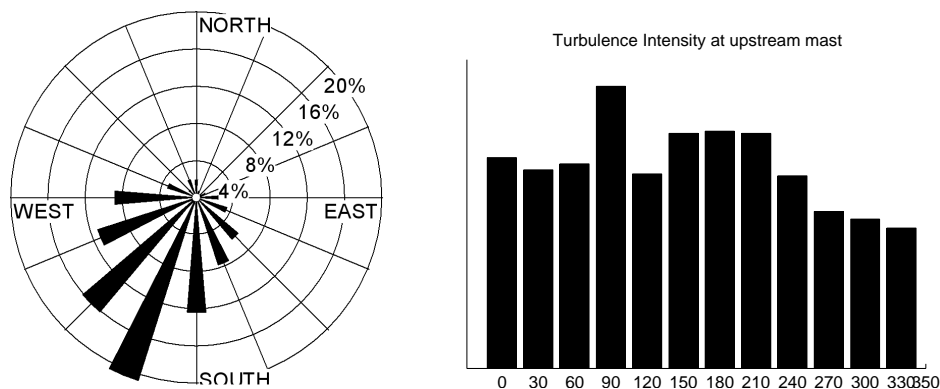


Figure 2. Left: The windrose measured at the upstream mast (M0) from December 2007 to March 2008. Right: Turbulence intensity measured at the upstream mast (M0) at 12 m height.

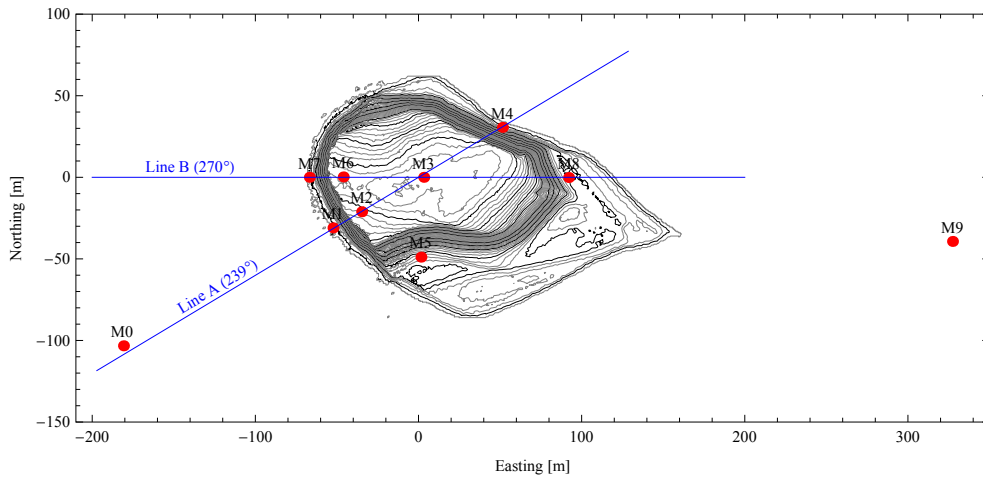


Figure 3. The Bolund orography and the mast positions along line A and B. The two lines cross the centerpoint of Bolund (CP) that is located close to Mast M3.

During the campaign, velocity and high frequency turbulence data were collected simultaneously from 35 anemometers distributed on the 10 masts. In total 23 sonics, 12 cups and 2 lidars were used. An overview of the instrumentation can be found in Table 1 and a description of the data acquisition and the anemometers can be found in Section 4.3-4.7. The "undisturbed" wind conditions were measured at mast M0 and M9 for winds from west and east, respectively (see Figure 3). Mast M0 and M9 were relative tall (~ 15 m) compared to the hill height (11.8 m) and were instrumented with both cup and sonic anemometers, thereby achieving a good estimate of the free stream wind conditions. Lidars, that measured the wind speed at heights up to 300 m supplemented these free stream measurements. Most masts were located along line A and B: M1, M2, M3, M4 along the 239° direction (line A) and M7, M6, M3, M8 along the 270° and 90° direction (Line B). A tenth mast, M5, was located independently from the others in a region where recirculating flow could be present. Except for mast M0 and M9, sonics were placed at 2 m and 5 m height in all masts along line A and B in order to achieve continuous measurements. The precise measuring positions are found in Section 4.8.

3D sonic anemometers formed the core of the instrumentation. The Mekttek USA-1 Basic sonic anemometer was used. This anemometer lacks a 3D correction found in the more expensive USA-1 Scientific model, but the correction can be applied offline to the data. This is described in Chapter 5. The final chapter (Chapter 6) describes the MySQL database and how the experimental data is stored. Examples of how to retrieve data is also given.

Table 1. Overview of the instrumentation used. The measuring heights are only approximate. The precise heights are given in Section 4.8. C - Cup anemometer, S - Sonic anemometer, L - Lidar.

Mast. ID	2m	5m	9m	15m	Lidar
M0	C	C,S	C	C	-
M1	S	S	S	-	-
M2	S	S	C,S	-	L
M3	S	S	C,S	-	-
M4	S	S	S	-	-
M5	S	S	-	-	-
M6	S	S	C	-	-
M7	S	S	-	-	-
M8	S	S	C	-	-
M9	C	C,S	C	C	L

3 Site Details

3.1 General Site Description

The Bolund experiment was initiated from a need for experimental data of the wind flow around complex terrain at atmospheric scale. The data set was needed to validate numerical flow models and to further increase our understanding of boundary layer flow, especially in connection with siting of wind turbines. Bolund is a peninsula located just north of Risø DTU National Laboratory for Sustainable Energy at Roskilde Fjord (Denmark). At first sight the 12 m high, 130 m long and a 75 m wide coastal hill does not seem like the ideal location for a measuring campaign. Bolund is certainly too small for a wind turbine site. If we for a moment, however, forget the actual size of Bolund, then we see that Bolund contains many appropriate characteristics for a complex terrain experiment:

- Complex 3D geometry, with well-exposed vertical escarpment
- Sharp change in surface roughness
- Uniform, well-defined surface roughness
- Isolated location with long upwind fetch from the sea
- Easily accessible from Risø DTU

All the above characteristics spoke in favor of using Bolund for a measurement campaign. The obvious downside of Bolund is the small size. Due to the size, the wind around Bolund lacks some of the large scale flow phenomena that exists at many wind turbine sites; thermal and Coriolis effects, for instance, have negligible effect on the local wind around Bolund. Instead of seeing the size of Bolund as a disadvantage it can actually be turned into an advantage. The lack of temperature and Coriolis effects can actually be seen as a benefit when validating numerical codes. Two effects that could influence the results have been avoided and a more well-defined validation is possible. Since the size of Bolund is sufficiently large for the flow to become Reynolds number independent the Bolund experiment can, in some extent, be seen as a scale-down experiment of a wind turbine site (scale effects are further discussed in Section 3.2). Based on these considerations Bolund was selected for the experiment. Being a place of natural beauty, Bolund is protected by the Nature Conservancy Board. Risø DTU was, however, able to secure time limited permissions from all official authorities and the local land owners for an experiment from December 2008 to February 2009.

Bolund is located approximately 1 km north of Risø DTU (see Figure 4) and the coordinates are (694682.098; 6177441.825) (UTM zone32, EUREF89, DVR90). In order to make coordinates more readable and avoid roundoff errors all coordinate values has been subtracted (694682.098; 6177441.825) in the following. We denote the origin the center point (CP). To the west there is a long fetch of sea of approximately 7 km (270°), while the fetch with the wind from west southwest (239°) is about 4 km. These directions are also the predominant wind directions (see Figure 2) and are the directions of most interest in the experiment. The terrain to the east consist of farmland with low rolling hills. At days of strong wind the sealevel rises due to pile up of water in Roskilde fjord. This is evident by the flooding of the isthmus that connects Bolund to the main land (see Figure 5). Since the water level changes up to 2 m, it has an affect on the flow around Bolund and needed to be measured during the campaign (see Section 4.2).

The west coast of Bolund consists of a small beach covered with small rocks (~ 20 cm) followed by the characteristic vertical cliff (see Figure 6). As the figure indicates, the leading edge between the cliff and the top of Bolund has a sharp nearly 90 degree crest. The top of Bolund consist of a flat well-defined plateau covered with grass. This plateau would have been suitable for a wind farm had it not been for the size of Bolund. The slopes of the northern, southern and eastern sides are also steep with slopes of up to 40 degree but here the crests are rounded.



Figure 4. Overview of Bolund from Google Earth.



Figure 5. Bolund from the east showing the isthmus connecting Bolund to the main land.



Figure 6. The west coast of Bolund seen from the south.



Figure 7. The northern and southern side of Bolund.

Except for the vertical escarpment and a narrow beach around the hill, Bolund is uniformly covered by grass (see Figure 7). Based on our experience evaluating ground roughness we suggest a roughness length of the Bolund surface of $z_0 = 0.015$ m. From the momentum flux measurements a value of $z_0 = 0.006$ m was estimated at M9 for easterly winds (see Section 6, example 2). However, since the measurements of z_0 are very uncertain and the grass on Bolund is longer than the grass to the east of M9 a value of $z_0 = 0.015$ m is recommended. The roughness length of the surrounding water is much lower. It can be described either as constant ($z_0 \approx 0.0003$ m) or by using the Charnock's approach [5], which relates the sea surface roughness and the friction velocity (u_*),

$$z_0 = \alpha_c \frac{u_*^2}{g}, \quad (1)$$

where $\alpha_c (\simeq 7 * 10^{-3})$ is a constant and g is the gravitational acceleration.

Most of the instrumentation used in connection with the experiment were deployed on masts located along two lines / directions through the hill's centerpoint CP. The two lines are designated line A (239° direction) and line B (270° direction) and are shown in Figure 8. The cross-sectional contour lines for line A and line B are seen on Figure 9, these have been extracted from the contour map (see Section 3.3). The cross-sectional contour lines show that the upstream and downstream escarpments for both directions are very steep. The downstream

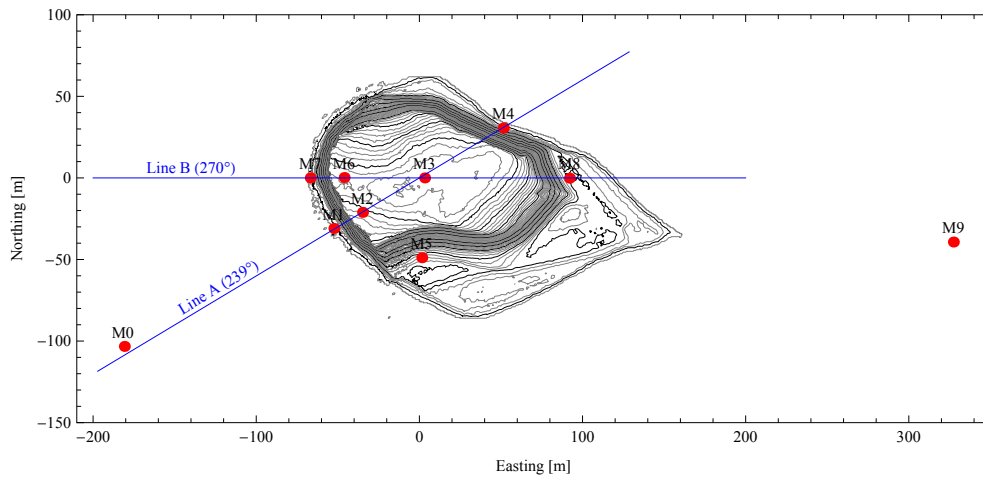


Figure 8. Position of masts

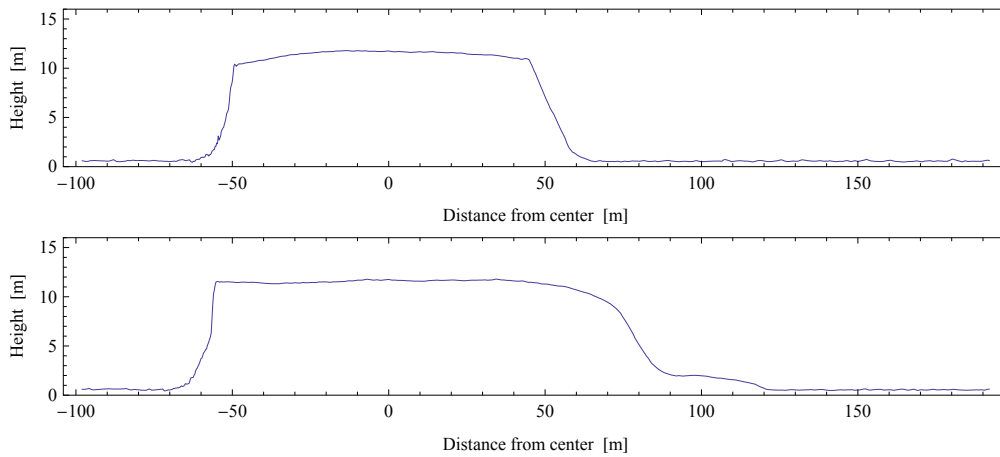


Figure 9. Cross-section of line A (top) and line B (bottom)

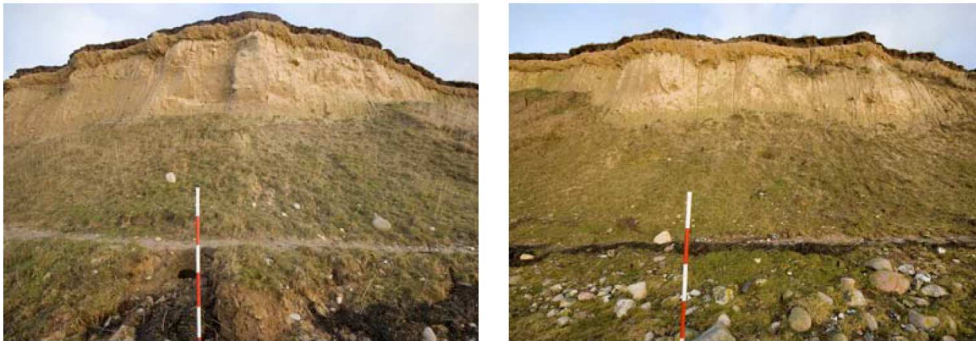


Figure 10. View from upstream of the escarpment. Left: line B (270 dir). Right: line A (239 dir).

slope (for westerly winds) for line A is almost vertical while the slope is more gentle for line B. On Figure 10 two photographs of the western escarpment is shown. Here it is seen that the escarpment crest is straight and perpendicular to the wind for line A, while it curves for line B. This subtle difference may have an influence on the flow and can be investigated by having masts deployed along both lines.

3.2 Scale Effects

Bolund is by all means a small hill: the maximum height of Bolund is 12 m, the length is approximately 150 m and the roughness length, z_0 varies from 0.3 mm over the water to 1.5 cm over the hill itself. In this section we want to compare Bolund with a Mesa hill, that is, a hill with physical dimensions 10 – 30 times larger than Bolund. Examples of such are often seen in Texas with wind turbines on the edge. We want to investigate whether the flow around Bolund is geometrically similar to that around a significantly larger hill of the same shape.

The geometry for the Mesa hill would be

$$h \rightarrow 120 - 360 \text{ m}$$

$$L \rightarrow 1.5 - 4.5 \text{ km}$$

$$z_0 \rightarrow 3.6 \text{ mm} - 0.45 \text{ m}$$

First we will look at the Reynolds number based on the hill height. For Bolund it is

$$Re_h \equiv \frac{Uh}{\nu} \sim \frac{10 \text{ m/s} \times 10 \text{ m}}{15 \cdot 10^{-6} \text{ m}^2/\text{s}} \sim 10^7. \quad (2)$$

This is very high and laminar flow can be ruled out. We can thus expect that the drag exerted by the hill on the flow has a constant drag coefficient independent of Reynolds number. A much higher Reynolds number as would be the case of the Mesa hill will therefore not change anything.

Instead of using the hill height, h , and the mean wind speed, U , we can instead construct a Reynolds number from the surface parameters: roughness length, z_0 and surface stress, u_* . Defined this way the Reynolds number says something about the surface turbulence relative to the viscosity. We thus compare the height, ℓ_i , of the layer mainly dominated by viscous effects and thus the layer where turbulence peaks for the two hills. [6] defined this layer for small hills, i.e. hills with $L \gg h$ and gentle slopes. In the literature this length is named the inner length, ℓ_i :

$$\ell_i \ln^2(\ell_i/L) = \alpha L \quad (3)$$

with $\alpha = 0.3$. For Bolund we get $\ell_i = 2$ m while we get $\ell_i = 21 - 63$ m for the Mesa hill, i.e. the exact 10 - 30 times used in the up-scaling. Due to the steepness of Bolund we might, however, expect ℓ_i to be larger.

A much more subtle effect from up-scaling Bolund to the Mesa hill is the influence of atmospheric stability and the height of the atmospheric boundary layer, z_i . In the case of Bolund, $h \ll z_i$ and $h \ll L$. The perturbations on the flow induced by the hill are thus more or less independent of stability effects and z_i . This means that we can treat the atmosphere as neutral. For the Mesa hill this might not work. In neutral situations where the wind speed is very high and in highly unstable situations, where z_i is very high everything is probably ok. In stable situations, where z_i tends to be very low and comparable with h strong effects of stratification are expected. The generalization from Bolund to the Mesa hill thus fails.

The last effects we will look at is the Coriolis force. For effects in the vertical direction we can repeat the arguments from above since the Ekman depth is more or less equal to the height atmospheric boundary layer. This means that the turning of the wind with height might interfere with the hill perturbations in at least stably stratified situations.

For the horizontal direction we look at the Rossby number:

$$Ro \equiv \frac{U}{fL}, \quad (4)$$

where f is the Coriolis parameter. $f \sim 10^{-4} \text{ s}^{-1}$ for mid latitudes. Using again $U \sim 10 \text{ m/s}$ we have for Bolund $Ro \sim 667$. This is much larger than one and Coriolis effects might therefore be neglected. For the Mesa hill, however, $Ro \sim 20 - 60$ and Coriolis effects might not that easily be neglected - independent of atmospheric stability.

The conclusion of this section is that even though Bolund is a small hill, in many respects it resembles the physics of a larger hill. The measurements done during the field campaign might therefore give us some insight into the realm of flows in complex terrain.

3.3 Contour Map

The map projection used for coordinates is the UTM (Universal Transverse Mercator) projection using the 6-degree longitudinal zone number 32 (UTM WGS84 zone 32). In order to make coordinates more readable and avoid roundoff errors all coordinate values has been subtracted CP=(694682.098; 6177441.825).

On February 1, 2007 the Bolund topography was scanned by COWI A/S using an airborne laser terrain mapper at 1600 m height (see appendix A for details on the instrument). The accuracy of

the measurements were about 15 cm vertically and 10 cm horizontally and a horizontal resolution of 2 m. The resulting "raw" measurement points (DTM-RAW-utm32-euref89-dvr90.xyz) were unstructured, i.e. they were not gridded. The horizontal resolution of the topography measurements was after inspection found inadequate to capture the vertical escarpment of Bolund, therefore additional measurements were performed. These were performed in the spring of 2008 using a high resolution laser scanner positioned on the beach in front of the escarpment. These measuring points (P57838A29MOHN-90000.xyz) were by COWI A/S placed in the same coordinate system.

In order to grid the measured data, the horizontal coordinates were first translated so that the new coordinate center was placed at (694682.098; 6177441.825). All the raw measuring points were then triangulated and based on this, a gridded file was generated with 25 cm resolution by linear interpolation. The water level around Bolund had dropped 0.30 m between the first and second topography scanning. In order to avoid a jump between the two dataset at the overlapping regions, the water level for the gridded file was set to 0.75 m. This additionally removed the water waves present in the first measurements.

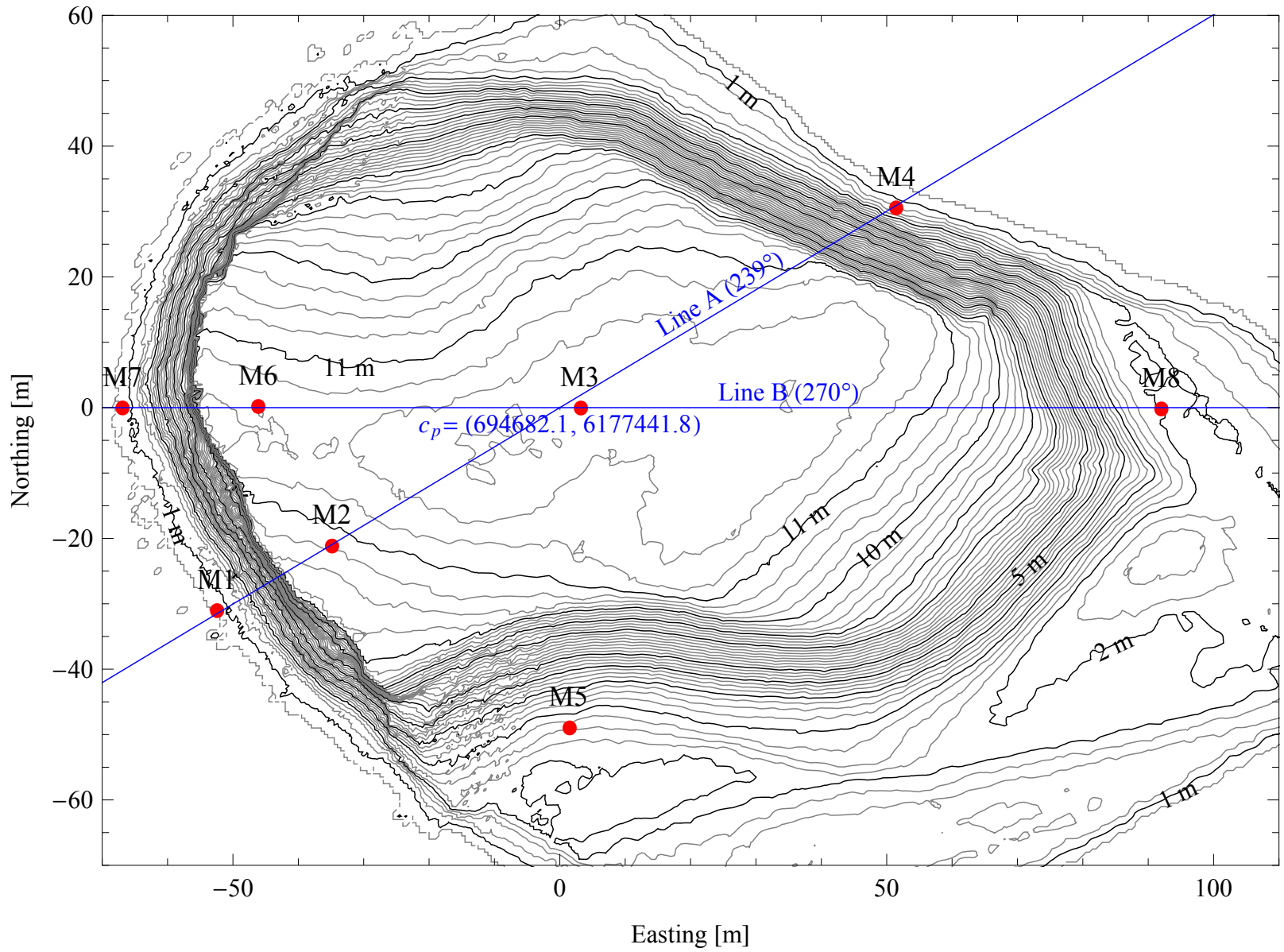
Another discrepancy between the two topography dataset, was the height of the vegetation. Except for the westerly beach and the vertical escarpment, Bolund is uniformly covered by grass. During the first topography scanning and the actual experiment the grass had a length of about 5 cm. At the time of the second scanning the height of the grass had grown to about 15 cm. Since the second scanning was focused on the vertical escarpment that was bare of grass the effect was here negligible. The northern and southern sides of Bolund were, however, covered with grass and here the slight height difference between the two dataset was seen as a sharp jump in the overlap region. Because of this, the 10 cm height difference between the two dataset was smoothed slightly in the two regions (the grass was cut). This was done by a simple linear transition between the two dataset over a length of 7 m.

Even though the gridded surface was quite uneven, especially around the vertical escarpment, only a minimum amount of smoothing have been applied to the dataset. Most of the unevenness represent resolved details of Bolund (rocks, grass etc.) that were captured during the second laser scanning. Ten sweeps with a gentle smoothing filter was however applied,

$$z_{i,j}^n = \frac{7}{8}z_{i,j} + \frac{1}{32}(z_{i+1,j} + z_{i-1,j} + z_{i,j+1} + z_{i,j-1}). \quad (5)$$

Instead of removing all the uneven details of Bolund the filter gently smoothen the small non-physical fluctuations otherwise present in the dataset. Users can apply their own smoothing filters for their specific application. The result was a gridded file of the Bolund topography with 25 cm resolution (Bolund.grd) and a gridded file (Bolund_roughness.grd) that contain the recommended values of roughness ($z_0 = 0.015$ m for Bolund and $z_0 = 0.0003$ m for the water). Using the program Matematica a map file containing 200 elevation contour lines and 1 roughness change line was made (Bolund.map). Together with a final file (Readme.txt) with a description of the data format, the four files represent the orography of Bolund.

Figure 11. The contour map of Bolund



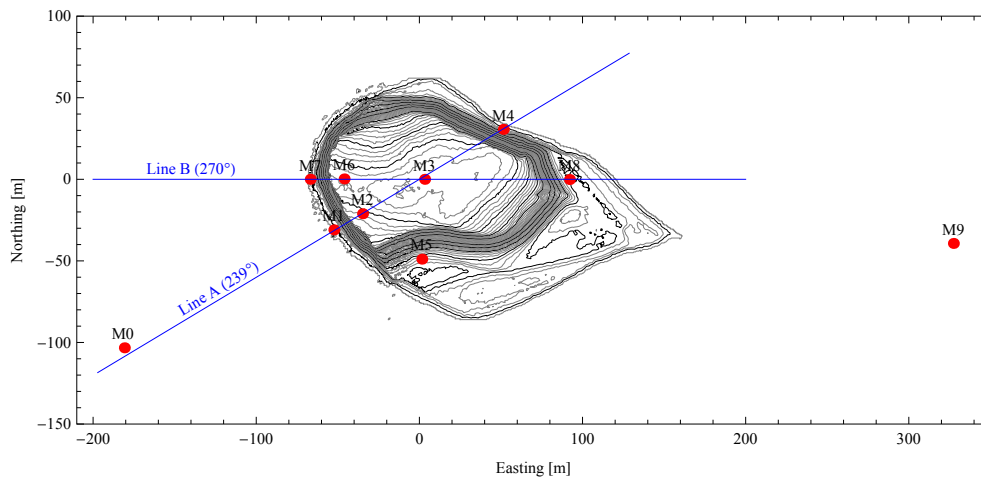


Figure 12. Position of masts

4 Experimental Setup

4.1 Overview

In [1] four regions of special interest were selected as regions where measurements should be performed: 1. upstream of the escarpment, 2. on the escarpment edge, 3. hill center and 4. in the hill wake. In order to accommodate these needs, a centerpoint (CP) of the hill was defined and masts were deployed along two lines through CP at the desired positions. The two lines, designated as line A (239° direction) and line B (270° direction) and the mast positions are shown in Figure 12. As seen, the mast designated M1, M2, M3, M4 are located along line A and M7, M6, M3, M8 are located along Line B. By having lines along two different flow directions, more experimental data was achievable during the measuring period. Additionally, the effect of escarpment geometry and the different cross-sectional contour lines can be investigated (see Section 3).

The "undisturbed" wind conditions was measured at mast M0 and M9 for winds from west and east respectively. Mast M0 and M9 were relative tall (~ 15 m) compared to the hill height (11.8 m) and were instrumented with both cup and sonic anemometers, thereby achieving a good estimate of the free stream wind conditions. Lidars, that measured the wind speed at heights up to 300 m, were placed at M9 and M2 (this Lidar was moved to M3 later on), to supplement the free stream measurements. Finally, a tenth mast, M5, was located independently from the others in a region where recirculating flow could be present. Cups were placed at the free stream masts in order to accurately measure the mean velocity profile and additional cups were placed at positions where wind inclinations were expected to be small [1]. The precise positions of the measuring masts and the instrumentation is found in the end of this section. Table 2 gives the horizontal distances from some relevant masts to CP projected onto the direction of line A and B. It should be noted that the positions of M3 and CP do not coincide.

Table 2. Horizontal distances in meters between CP and instruments on the masts projected onto the direction of Line A and Line B.

Line A	-208.2 (M0)	-60.9 (M1)	-40.7 (M2)	2.8 (M3)	59.9 (M4)
Line B	-180.8 (M0)	-66.9 (M7)	-46.1 (M6)	3.2 (M3)	92.0 (M8)

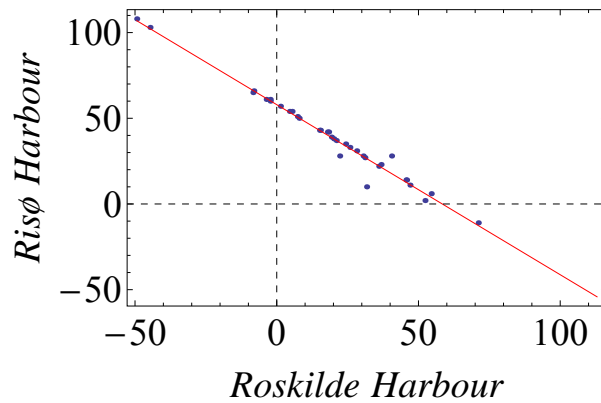


Figure 13. Correlation between water level measurements at Roskilde and Risø harbour

4.2 Water Level

Mast M0 was placed in the sea on a platform firmly positioned on the sea bed (see Figure 18). During the experiment the water level changed and consequently changed the measurement height on M0 and the actual hill height. It was therefore important to get accurate measurements of the water level.

An instrument was placed on the platform to measure the water level but the instrument never functioned properly (MySQL ID: Water_level). Instead it was chosen to rely on measurements performed in the harbor of the nearby city of Roskilde. Figure 13 shows the 10 minute averaged water levels (in centimeters) from Roskilde harbour as function of the water level at the Risø DTU harbour (located next to Bolund). The measurements from Risø was measured manually once a day during the experiment. As seen on the figure the two series are almost perfectly anti-correlated (opposite sign convention between the two harbours) (regression line: $f(x) = 57.94 - 0.99x$, $r^2 = 0.98$). This justifies the use of the Roskilde harbour measurements.

On figure 14 the Roskilde measurements is shown as a red curve while the measurements from Risø are shown as black dots. The three red dots are manual measurements of the platform height above water level. It is found that the difference between the platform height and the water level at Risø is ~ 57 cm. Ultimately, the regression function that transforms the water level measurements at Roskilde harbour into the platform height is $f(x) = 115 - 0.99x$, which is plotted as the green line on figure 14. The resulting 10 minute platform height has been stored in the MySQL database in the table platformheight (see Section 6).

On February 1 2007 at 0840 UTC the Bolund topography and surrounding water was scanned with an airborne laser terrain mapper. In the global coordinate system used, the mean water level at the time of scanning was $z=0.60$ m. In order to remove the water waves present in the measurements the water level for the topography files was increased to 0.75 m. The platform height at time of scanning was 45 cm which reduces to 30 cm in the final topography maps. To summarize, users that wants to extract measurements suited for the official map where the water level has been set to 0.75 cm should select data where the platform height is 30 cm.

4.3 Data Acquisition

Regarding data acquisition, the requirement for the Bolund experiment was to collect simultaneous data from around 60 sensors, distributed in 10 different locations, separated by distances of up to 1 km. Data should be sampled at the rate of 20 Hz. Due to the proximity of Risø DTU, our wish was also that the actual data storage should occur on our premises.

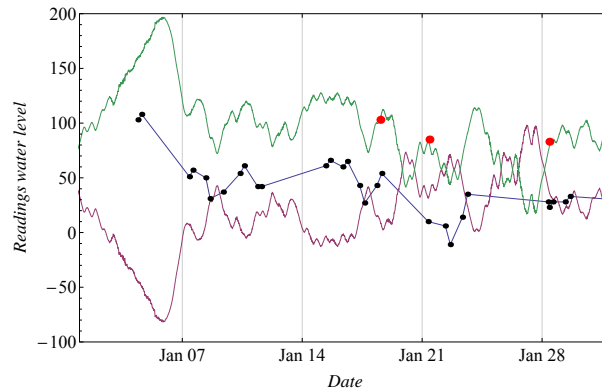


Figure 14. Red curve: 10 minute averaged water level measurements from Roskilde harbour. Black dots: water level measurements from Risø harbour. Red dots: water level to platform measurements. Green curve: the resulting platform height based on the measurements at Roskilde harbour.

The instrumentation consisted of over 20 sonic anemometers, 10 cup anemometers and a number of sensors for the climatological parameters such as temperature and humidity. In essence, all the sensors are registered from serially transmitted data telegrams. For the sonic anemometers, this is the intrinsic data format. Cup anemometers and analogue sensors are converted using a DAU (Risø P2858B), which outputs the registered data as a serial string.

Whereas normally a number of serial connections are made to a central data acquisition computer using a multi-port adapter, we adopted a new approach in which the serial telegrams are instead transmitted across a network. This gives the freedom to allow a number of de-central hubs where the serial to network conversion is made. Using a combination of optical and wireless network, the telegrams were transmitted to the central measurement computer, located in a laboratory at Risø DTU. As supplementary instrumentation, we used 2 lidars. These also made use of the network for transmitting data and permitting remote access for setup and inspection.

A diagram drawing of the complete experimental setup is found in appendix B

4.4 Sonic Anemometers

3D sonic anemometers formed the core of the instrumentation for the Bolund experiment. These were chosen because of the predominantly 3D nature of the flow fields. Sonic anemometers were selected for all the measuring points where significantly non-zero flow tilting was expected. The Metek USA1-Basic sonic anemometer was chosen. This is a relatively inexpensive, 3D sonic anemometer that has been used for many years at Risø DTU. The Metek sonic (see Figure 15) has one central strut rather than the more conventional outer bar design. This reduces the effects of flow distortion. Wind speed components and virtual temperature are output at rates up to 25 Hz. A generic head flow correction, based on the direction of the incoming flow, is implemented in the sonic's processor. We choose to select this head correction so that the recorded data were correct to a first approximation. A more sophisticated, 3D head correction, using both the wind direction and the flow tilt angle relative to the probe, is available in the more expensive USA-1 Scientific model. However, this correction can be applied offline to the data from the USA-1 Basic model, as described in Section 5. In the MySQL database and in the following the individual Sonic.id (MySQL ID) are constructed by the mast number and approximate measuring height, e.g. the sonic (S) placed at 2 meters height at mast M1 is called M1_S.2. The sonic data in the database are arranged according to two primary keys, Sonic.id and Name, where Name represents the time stamp in the format `yyyymmddhhmm`.



Figure 15. Left: The Metek Sonic. Right: The cup anemometer.

4.5 Cup Anemometers

For measuring wind in locations where little tilting of the flow was expected, e.g. on the offshore, upstream mast, traditional cup anemometers have been used. We have selected the Wind-Sensor P2546 ('Risø') cup anemometer. This is a Class 1 cup anemometer, according to the IEC 61400-12 classification [7]. Classification documents, including details of the angular response, can be found at <http://www.cupanemometer.com/products.htm>. The design originates from Risø National Laboratory and is currently manufactured under license by WindSensor. It is a relatively fast responding instrument with a length constant of 1.8m. Two pulses per revolution are generated, using a Namur type switch, activated by a 2 pole magnet fixed to the rotating anemometer shaft. For each cup anemometer, the period of the pulse train is determined in a DAU (Risø P2858B) and the reciprocal of this period (the frequency, proportional to the wind speed) is added to the output telegram. Each cup anemometer was calibrated prior to the campaign, according to the prevailing Measnet standard [8]. The name convention (MySQL ID) for the cups are similar to the sonics, e.g. a cup placed at 2 meters height at mast M0 is called M0_Cup.2.

4.6 Temperature

Temperature and temperature difference were measured using several different sensor types. Absolute temperature (air and water) was sensed using a Pt100 sensor (Risø P2449A). The absolute air sensor (MySQL ID: T0_Tabs.2) used a passive radiation screen (Risø P2029) whilst the water temperature sensor (MySQL ID: M0_TWATER) had no screen. Air temperature gradient was measured using a paired set of two Pt500 sensors, with the difference signal from these two probes derived using the Risø P1867A Temperature Gradient Transmitter. This is a direct measurement of the temperature difference. The two sensors were screened using a P2029 passive radiation screen. One pair of sensors was mounted on the offshore platform (M0) measuring the gradient between 12m and 2m (MySQL ID: M0_Tdiff_12_2), the other pair at mast M1 measuring the gradient between 9m and 2m (MySQL ID: M1_Tdiff_9_2). In both cases a temperature increasing with height is indicated by a positive value. The surface temperature of the water (MySQL ID: T_surf) was measured using a passive, infra-red sensor (Heimann F2362A) staring down at the water surface. This was mounted on the offshore, upstream platform.



Figure 16. Left: Lidar positioned close to mast M2. Right: Lidar by mast M9. (The photograph looks distorted due to the use of wide angle lens).

4.7 Lidar

Traditional point wind measurements (cup and sonic anemometers) were supplemented by lidar profiler measurements. The purpose of this was twofold; firstly to provide an upstream wind speed profile to significantly higher heights than the available meteorological mast; secondly to provide datasets of lidar measurements in complex terrain that could be used to further investigate how to interpret such data. Lidar measurements were made using two ZephIR lidars. The ZephIR is a continuous wave (cw) lidar that uses a variable focus to interrogate successive heights. Each height is conically scanned for one or three seconds, after which the horizontal speed is recovered from the set of radial speeds obtained for the different azimuth directions. Up to five heights are scanned successively, a complete cycle taking up to 18 seconds. ZephIRs have been commercially available since 2006 and it is estimated that well over 50 units are in operation. The design is described in greater detail in [9]. One ZephIR (MySQL ID: Unit 2) was placed close to M9 (about 10m to the south). The purpose of this system was to provide a reference profile to greater heights than permitted by the mast measurements. Although ideally this system would have been best located on the offshore platform, such a deployment was considered to be too risky and logistically demanding. For wind directions with a water fetch at M9, it is anticipated that the reference profile measured here and at the offshore platform would not be significantly different. This assumption has not yet been rigorously validated. The second ZephIR (MySQL ID: Unit 102) was placed on the Bolund hill at 2 different locations with varying complexity. From January 28, to February 15, 2008 this lidar was located 8.5m south of M2, very close to the shear face of the escarpment (4.2m from the escarpment). It can be expected that the horizontal speeds reported by the lidar in this position are strongly affected by the inhomogeneity of the flow. From February 15, 2008 (1540) until February 25, ZephIR unit 102 was operating 10m south of M3, in the centre of the hill. In this position the degree of inhomogeneity is less and we expect better agreement between the horizontal speeds measured by the lidar and the mast instrumentation.

As an example, the wind speed measured by the lidar close to mast M9 on the isthmus at a height of 14 m above the instrument is compared to the cup anemometer speed at 15.6 m above the ground at the same mast. Figure 17 shows that the lidar underestimates the cup speed by less than 3% with very little scatter. The MySQL query used to extract these data is shown in section 6. The situation is quite different when comparing the lidar with the cup at mast M2 close to the cliff. Here the lidar underestimates the horizontal wind speed relative to the cup with 7.5%. The reason is that here the flow is not horizontally homogeneous, which is assumed in deriving the horizontal wind speed from the conical scan performed by the lidar. A thorough analysis of this difference is discussed in [10].

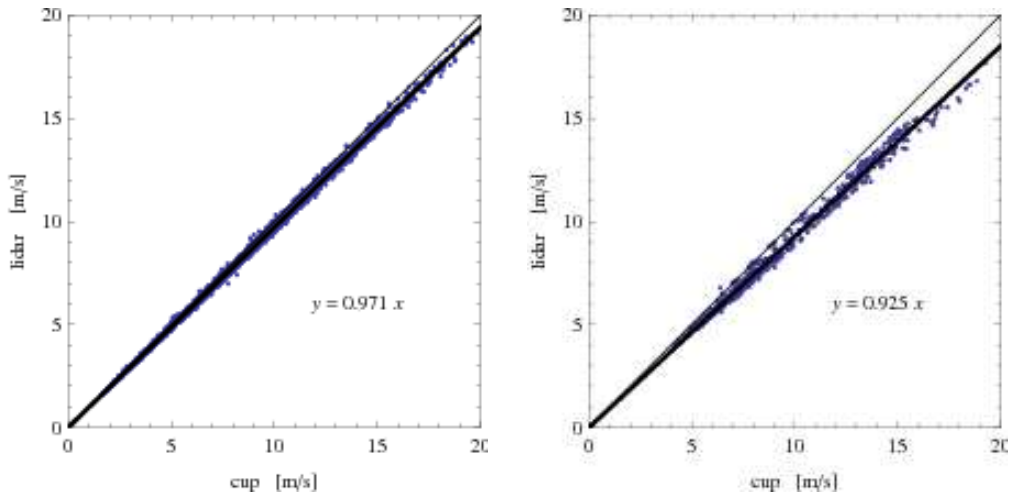


Figure 17. Left: Comparison of the horizontal wind speed measured at mast M9 at 15 m with a cup anemometer versus with a lidar as the same height. Right: Comparison at mast M2 at 11 m above the ground.

4.8 Measuring Positions and Instrumentation ID

The positions of the ten masts are given in Table 3. The position were measured by Risø DTU and confirmed by additional measurements performed by MOLBAK landinspektører A/S on January 16, 2008. The instruments were placed on 1.8m long booms that for most cases were directed south (see Table 17 for boom directions). Table 4 gives these positions i.e. the positions of the instruments on the masts. The terrain height given in Table 4 was found from the topography file (Bolund.grd).

The boom positions was carefully placed at the desired heights and were remeasured by MOLBAK landinspektører. An uncertainty on the measured heights of no more than ± 20 cm is expected. Below are tables showing the positions of the individual instruments. In subsequent tables the measuring positions and heights for the individual instruments are also shown. Additionally, the instrumentation ID used in the MySQL database is given.

Table 3. The table gives the mast positions. The water level changed during the experiment, however the recommended water level of 0.75m is used in the table

Mast ID.	x (E) [m]	y (N) [m]	Ground level [m]
M0	-181.7	-101.7	0.8
M1	-52.5	-29.2	0.8
M2	-34.9	-19.3	11.0
M3	3.1	1.8	11.7
M4	51.5	32.4	0.9
M5	1.3	-47.1	2.9
M6	-46.2	2.0	11.4
M7	-66.9	1.8	0.8
M8	92.0	1.7	2.0
M9	327.3	-37.5	1.4

Table 4. The positions of the mast anemometers. The instruments were placed on 1.8m long booms that for most cases were directed south. This table shows these positions.

Mast ID.	x (E) [m]	y (N) [m]	Ground level [m]
M0	-180.8	-103.3	0.8
M1	-52.4	-31.0	0.8
M2	-34.8	-21.1	10.8
M3	3.2	0.0	11.7
M4	51.5	30.6	1.4
M5	1.5	-48.9	2.6
M6	-46.1	0.2	11.5
M7	-66.9	0.0	0.8
M8	92.0	-0.1	2.00
M9	327.3	-39.3	1.4

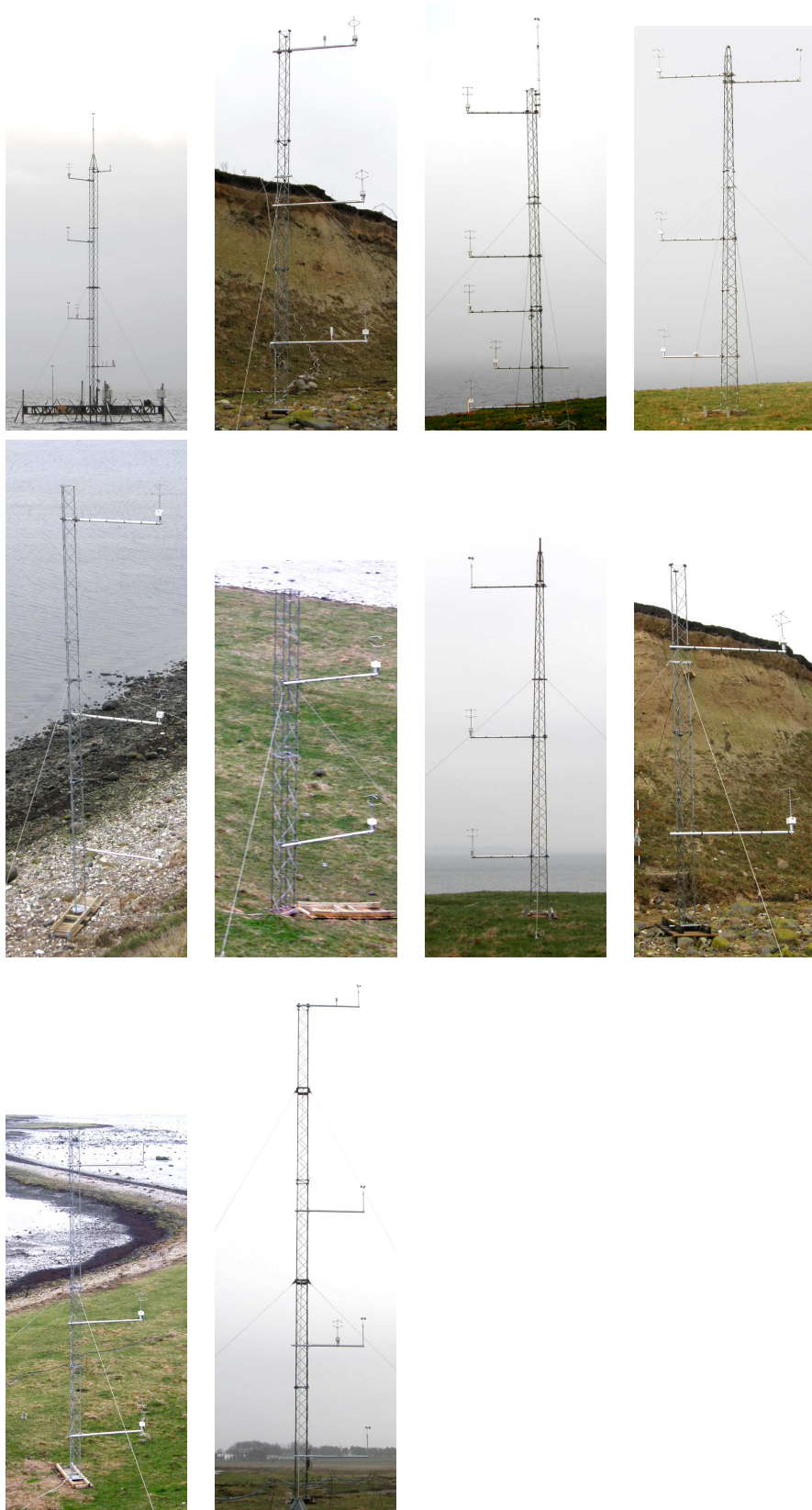


Figure 18. The ten measuring masts used, counting from left to right. Mast 0 is top left and mast 3 top right

Table 5. Instrumentation of Mast 0. The mast was placed at sea on a platform. z_{apl} is the height above the platform and z is the height in the global coordinate system. In the topography files the water level is set to $wl = 0.75\text{m}$. Instrument height above water level is found by $z_{awl} = z - wl$. The water level measurements from this platform are unreliable (see Section 4.2). There is no water temperature measurements from about 030108 to 080108. In this period, the water level was very low and the instrument was in the air.

Instr. ID	z_{apl} [m]	x [m]	y [m]	z [m]	Start	End
M0_Cup_2	2.0	-183.5	-102.7	3.1	211207	250208
M0_Cup_5	5.0	-180.8	-103.3	6.1	211207	250208
M0_Cup_9	9.0	-180.8	-103.3	10.1	211207	250208
M0_Cup_15	15.0	-181.7	-101.7	16.1	211207	250208
M0_S_5	5.0	-181.3	-102.5	6.1	211207	250208
M0_S_12	12.0	-180.8	-103.3	13.1	100108	250208
M0_Tabs_2	2.0	-180.8	-103.3	3.1	211207	250208
M0_Tdiff_12_2	2.0-12.0	-180.8	-103.3	3.1-13.1	211207	250208
M0_Tsurf	-	-180.8	-103.3	-	211207	250208
M0_TWater	-	-180.8	-103.3	-	211207	250208
Waterlevel	-	-180.8	-103.3	-	211207	250208

Table 6. Instrumentation at mast 1. z_{agl} is the height above ground. x, y and z are the coordinates in the global coordinate system. Start and End indicates the measuring period for that specific instrument

Instr. ID	z_{agl} [m]	x [m]	y [m]	z [m]	Start	End
M1_S_2	2.1	-52.4	-31.0	2.8	211207	250208
M1_S_5	5.1	-52.4	-31.0	5.8	211207	250208
M1_S_9	9.0	-52.4	-31.0	9.8	211207	250208
M0_Tdiff_9_2	2.1-9.0	-52.9	-29.2	2.8-9.8	211207	250208

Table 7. Instrumentation at mast 2. z_{agl} is the height above ground. x, y and z are the coordinates in the global coordinate system. Start and End indicates the measuring period for that specific instrument. The cup at 9 meters height was changed to 11 meters at 240108. At that time a new sonic was placed at 9 meters height. A new sonic was also placed at 3.6 meters height at 140108.

Instr. ID	z_{agl} [m]	x [m]	y [m]	z [m]	Start	End
M2_Cup_9	9.1	-34.8	-21.1	19.9	211207	240108
M2_Cup_11	11.1	-34.9	-19.3	21.9	240108	250208
M2_S_1	1.1	-34.8	-21.1	11.9	211207	250208
M2_S_2	2.1	-34.9	-20.2	12.9	211207	250208
M2_S_3	3.6	-34.8	-21.1	14.4	140108	250208
M2_S_5	5.1	-34.8	-21.1	15.9	211207	250208
M2_S_9	9.1	-34.8	-21.1	19.9	240108	250208
Zephir unit 102	0.0	-34.8	-27.8	10.8	280108	150208

Table 8. Instrumentation at mast 3. z_{agl} is the height above ground. x, y and z are the coordinates in the global coordinate system. Start and End indicates the measuring period for that specific instrument

Instr. ID	z_{agl} [m]	x [m]	y [m]	z [m]	Start	End
M3_S_9	9.0	3.1	3.6	20.6	211207	250208
M3_S_2	2.0	3.2	0.0	13.6	211207	250208
M3_S_5	5.0	3.2	0.0	16.6	211207	250208
M3_S_9	9.0	3.2	0.0	20.6	240108	250208
Zephir unit 102	0.0	3.2	-10.0	11.7	150208	250208

Table 9. Instrumentation at mast 4. z_{agl} is the height above ground. x, y and z are the coordinates in the global coordinate system. Start and End indicates the measuring period for that specific instrument

Instr. ID	z_{agl} [m]	x [m]	y [m]	z [m]	Start	End
M4_S_2	1.4	51.5	30.6	2.8	211207	250208
M4_S_5	4.4	51.5	30.6	5.8	211207	250208
M4_S_9	8.4	51.5	30.6	9.8	211207	250208

Table 10. Instrumentation at mast 5. z_{agl} is the height above ground. x, y and z are the coordinates in the global coordinate system. Start and End indicates the measuring period for that specific instrument. The instruments was removed ta 240108 and used at the other masts

Instr. ID	z_{agl} [m]	x [m]	y [m]	z [m]	Start	End
M5_S_2	2.2	1.5	-48.9	4.8	211207	240108
M5_S_5	5.2	1.5	-48.9	7.8	211207	240108

Table 11. Instrumentation at mast 6. z_{agl} is the height above ground. x, y and z are the coordinates in the global coordinate system. Start and End indicates the measuring period for that specific instrument

Instr. ID	z_{agl} [m]	x [m]	y [m]	z [m]	Start	End
M6_Cup_9	8.9	-46.1	0.2	20.4	211207	250208
M6_S_2	1.9	-46.1	0.2	13.3	211207	250208
M6_S_5	4.9	-46.1	0.2	16.4	211207	250208

Table 12. Instrumentation at mast 7. z_{agl} is the height above ground. x, y and z are the coordinates in the global coordinate system. Start and End indicates the measuring period for that specific instrument

Instr. ID	z_{agl} [m]	x [m]	y [m]	z [m]	Start	End
M7_S_2	2.0	-66.9	0.0	2.8	211207	250208
M7_S_5	5.0	-66.9	0.0	5.8	211207	250208

Table 13. Instrumentation at mast 8. z_{agl} is the height above ground. x, y and z are the coordinates in the global coordinate system. Start and End indicates the measuring period for that specific instrument

Instr. ID	z_{agl} [m]	x [m]	y [m]	z [m]	Start	End
M8_Cup_9	8.8	92.0	-0.1	10.8	211207	250208
M8_S_2	1.8	92.0	-0.1	3.8	211207	250208
M8_S_5	4.7	92.0	-0.1	6.8	211207	250208

Table 14. Instrumentation at mast 9. z_{agl} is the height above ground. x, y and z are the coordinates in the global coordinate system. Start and End indicates the measuring period for that specific instrument

Instr. ID	z_{agl} [m]	x [m]	y [m]	z [m]	Start	End
M9_Cup_2	1.9	327.3	-39.3	3.3	211207	250208
M9_Cup_5	5.0	327.3	-39.3	6.4	211207	250208
M9_Cup_9	9.0	327.3	-39.3	10.4	211207	250208
M9_Cup_15	15.6	327.3	-39.3	17.0	211207	250208
M9_S_5	5.0	327.3	-38.4	6.4	211207	250208
Zephir Unit 2	0.0	327.3	-49.3	1.4	211207	250208
M9_Tdiff_14_2	1.9-14.0	327.3	-39.3	3.3-15.4	231207	250208

5 Sonic Data Processing

This section describes the sonic measurements in the Bolund campaign from the 21. of December 2007 to the 25. of February 2008. The different measurement periods are recollected in Table 15. In each period a different number of sonics were mounted. The different sonic heights and masts of each period can be seen in Table 16. Sonics of type Metek USA-1 (Basic) were used. We have corrected the obtained velocities and temperature for 3D flow distortion and constructed 10min and 30min statistics in different coordinate systems. The final results are stored in the Risø MySQL database.

5.1 Metek3d Corrections

Flow distortion by the presence of the sonic themselves induces systematic errors in the recorded data, and only distortion in the azimuthal angle has been corrected in the online sonic recordings. We have therefore also corrected all data for the flow distortion due to the tilt of the flow field. The approach is based on look-up tables provided by Metek (See Appendix C).

The raw measured 20Hz data are stored in the databases **bolund.caldata_x_20hz** (see Section 6.2), where **x** runs from 1 to 4 referring to the four measurement periods. Data are stored as 4 byte floating point values. The corresponding corrected data are stored in **bolund.metek3dcorr_x_20hz**, where **x** again runs from 1 to 4. Data are here stored as 2 byte integer values and in units of $1/100(m/s \text{ or } ^\circ C)$. In general, all tables in the MySQL database **bolund** referring to corrected data will have the string **metek3dcorr** included in the title.

Table 15. Dates are denoted *yyyymmddhhmm*. The coverage represent the percentage of mean records (of 10 min and 30 min respectively) constructed out of the full duration of the period. The number is averaged over all sonics mounted in the period.

period	start	end	duration	coverage - 10min/30min
1	200712211620	200801101440	19d22h20m	95.9% / 95.2%
2	200801101500	200801141240	03d21h40m	97.1% / 95.2%
3	200801141300	200802112140	28d08h40m	85.7% / 84.8%
4	200802121540	200802250850	12d17h10m	92.7% / 89.1%

Table 16. Table of sonics mounted at mast with *id = MX* and height position *Xm* above terrain. The different numbers corresponds to the different periods. The precise measuring heights can be found in Tables 5-14. *Period starts at 20080124.

	1m	2m	3.5m	5m	9m	12m
M0	-	-	-	1234	-	234
M1	-	1234	-	1234	1234	-
M2	1234	1234	34	1234	34*	-
M3	-	1234	-	1234	34*	-
M4	-	1234	-	1234	1234	-
M5	-	12	-	12	-	-
M6	-	1234	-	1234	-	-
M7	-	1234	-	1234	-	-
M8	-	1234	-	1234	-	-
M9	-	-	-	1234	-	-

5.2 Velocity corrections

For velocity correction, the approach is straight forward. First we remove the 2D correction, which was added online when recording. Hereafter, the 3D correction is added. If we let (u_c, v_c, w_c) denote the 2D corrected velocity components and (u_r, v_r, w_r) be the uncorrected (raw) velocity components the transformation is given by [11]:

$$u_r = u_c / \delta \quad (6)$$

$$v_r = v_c / \delta \quad (7)$$

$$w_r = w_c - 0.031 s_c \sin(3\alpha_r - 1) / \delta, \quad (8)$$

where s_c is the 2D corrected horizontal speed, $s_c = \sqrt{u_c^2 + v_c^2}$ and α_r is the raw wind direction, $\alpha_r = -\tan^{-1}(u_r, v_r)$, where the function $\phi = \tan^{-1}(x, y)$ takes into account which quadrant the point (x, y) is in, such that $x = \sin(\phi)$ and $y = \cos(\phi)$. The correction factor δ is given by

$$\delta = 1 + 0.015 \sin(3\alpha_r + \pi/6). \quad (9)$$

The correction is displayed in Figure 19. The uncorrected raw velocities, (u_r, v_r, w_r) are corrected for 3D flow distortion. That is distortion due to tilt is also considered. This, as we will show, is crucial for our flow situation since the orography and hence flow lines are far from horizontal around the edges of Bolund. The correction is again given by [11], this time through look-up tables. These tables have been generated from experiments in a wind tunnel. This, on the other hand, means that the corrections does not necessarily work optimally for atmospheric purposes as ours. We have therefore multiplied the corrected speed with a factor $\beta = 0.975$ (Troels Petersen, personal communication) in order to restore a number of physical properties of atmospheric turbulence (see plots later). This time we let $\bar{u}_c = (u_c, v_c, w_c)$ denote the correction velocity, such that

$$\bar{u}_0 = \bar{u}_r + \bar{u}_c(\bar{u}_r) \quad (10)$$

where $\bar{u}_0 = (u_0, v_0, w_0)$ is the 3D corrected and hence desired velocities from which all statistics will be calculated. Metek assumes further that \bar{u}_c is solely determined by \bar{u}_r and that the linear

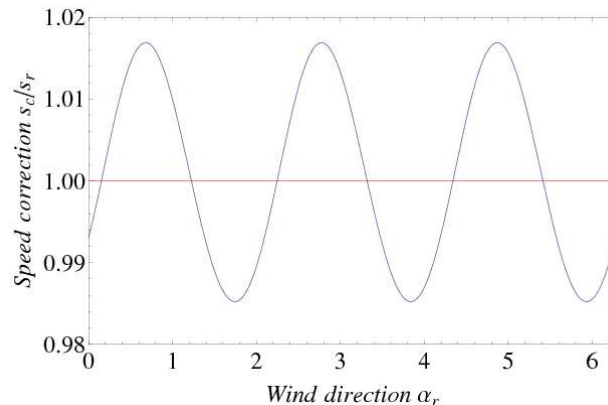


Figure 19. Normalized 2D correction.

law $\bar{u}_r(t\bar{u}_0) = t\bar{u}_r(\bar{u}_0)$ is valid for a given scalar t . Wind tunnel experiments have established this relationship. Like in the 2D case we define polar coordinates with wind speed given by $s = |\bar{u}| = \sqrt{u^2 + v^2 + w^2}$, wind direction $\alpha = \tan^{-1}(-u, -v)$ and tilt $\phi = -\tan^{-1}(\sqrt{u^2 + v^2}, w)$. The angles, α and ϕ are here defined a little different than usual. The definition here differs from the ones given in [11] but is necessary in order to utilize the look-up tables correctly. The recipe is straight forward:

1. The raw velocities (u_r, v_r, w_r) are transformed to the polar coordinates (s_r, α_r, ϕ_r) .
2. The following corrections are made:

$$s_0 = s_r(1 + n_c(\alpha_r, \phi_r)) \quad (11)$$

$$\alpha_0 = \alpha_r + \alpha_c(\alpha_r, \phi_r) \quad (12)$$

$$\phi_0 = \phi_r + \phi_c(\alpha_r, \phi_r) \quad (13)$$

3. Transformation of polar coordinates back to the desired 3D corrected velocities (u_0, v_0, w_0) :

$$u_0 = -s \cos(\alpha_0) \cos(\phi_0) \quad (14)$$

$$v_0 = -s \sin(\alpha_0) \cos(\phi_0) \quad (15)$$

$$w_0 = -s \sin(\phi_0) \quad (16)$$

The three correction functions $n_c = s_c/s_r = n_c(\alpha_r, \phi_r)$, $\alpha_c(\alpha_r, \phi_r)$ and $\phi_c(\alpha_r, \phi_r)$ are given by Fourier series with coefficients $C_{f,i}(\phi_r)$ and $S_{f,i}(\phi_r)$ from look-up tables:

$$f_c(\alpha_r, \phi_r) = \sum_{i=0,3,6,9} (C_{f,i}(\phi_r) \cos(i\alpha_r) + S_{f,i}(\phi_r) \sin(i\alpha_r)) \quad (17)$$

where $f_c(\alpha_r, \phi_r)$ is one of the three correction functions. The look-up tables for $C_{f,i}(\phi_r)$ and $S_{f,i}(\phi_r)$ are given in steps of 5° ranging from -50° to $+45^\circ$ of the measured flow angle ϕ_r . Linear interpolation is used between tabulated values. The coefficients are given in the appendix. The factor $\beta = 0.975$ should be multiplied onto the values given in the sine and cosines look-up tables for $n_c(\alpha_r, \phi_r)$. The wind direction and tilt angle are left unchanged.

In the left panels of Figure 20 the 3D correction on speed, wind direction and tilt as a function of uncorrected wind direction and tilt are presented. We see that the corrections are quite large, a couple of degrees. The total corrections, that is after subtraction of the 2D correction and addition of the 3D correction, are presented in the right panels of Figure 20. Especially for the tilt we see that the total correction increases with measured tilt (2D corrected).

5.3 Temperature corrections

From the sonics we can also obtain the temperature since the speed of sound is mainly a function of the local temperature. The velocity of sound is thus approximated as $c^2 = 403T$, where c is the sound speed and T is the local temperature. Including a cross wind and defining the temperature as a mean over all three paths the correction to the temperature is according to [12] $1/403$ times the mean square of the normal velocity on the three paths. The arrangement of the of the three paths between the sonic heads can be expressed by the matrix,

$$M = \begin{pmatrix} \sin(\phi) & 0 & \cos(\phi) \\ -\frac{\sin(\phi)}{2} & \frac{1}{2}\sqrt{3}\sin(\phi) & \cos(\phi) \\ -\frac{\sin(\phi)}{2} & -\frac{1}{2}\sqrt{3}\sin(\phi) & \cos(\phi) \end{pmatrix} \quad (18)$$

with row M_i representing the i 'th path. The pre-factors have been determined from assuming a spacing of 120° between the sonic heads. ϕ is the angle of the acoustic paths relative to vertical,

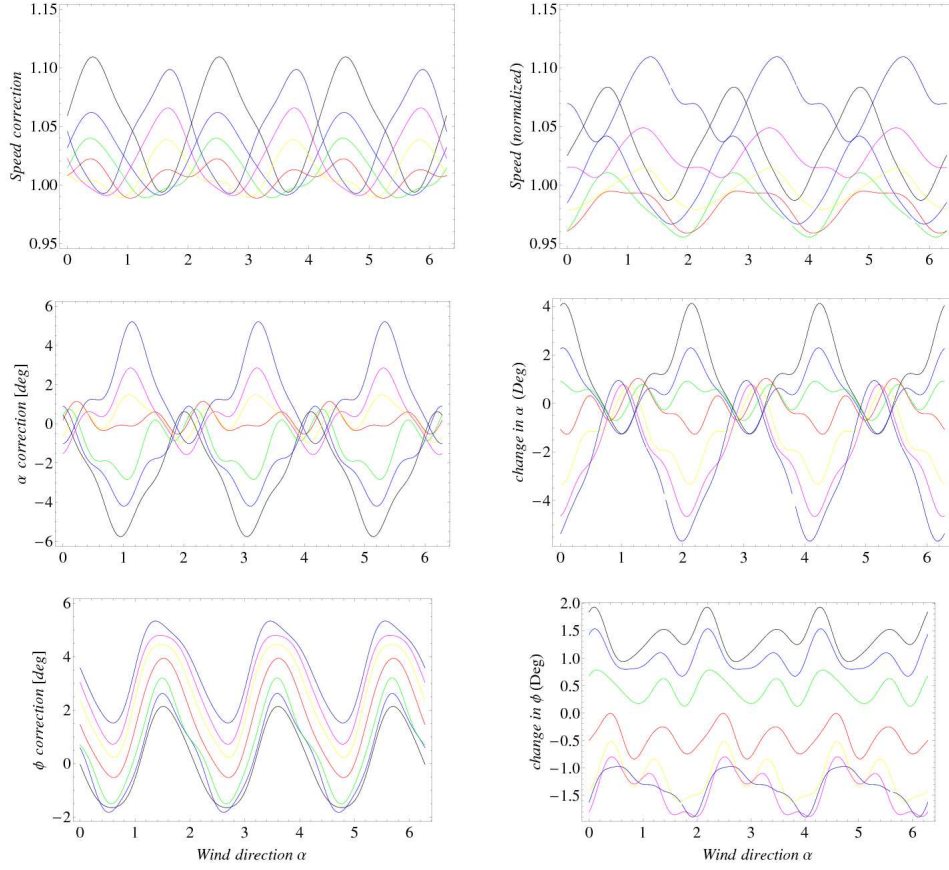


Figure 20. The top figures show normalized speed whereas the middle figures shows change in wind direction α and the bottom figures show change tilt angle ϕ - all as function of measured wind direction α_r . left: 3D correction only, right: total correction: the 2D correction has first been subtracted after which the 3D correction has been added. The different colors represent different value of ϕ : $\{-15^\circ$: Black, -10° : Blue, -5° : Green, 0° : Red, 5° : Yellow, 10° : Magenta, 15° : Dark Blue}

and it is 45° for the METEK sonics. According to [12] we need to find the mean square of the normal velocity, \bar{V}_n , on the three paths. This is done by projecting each sonic path onto the cross wind:

$$\frac{1}{3} \sum_i^3 |\bar{u} - (\bar{u} \cdot M_i) M_i|^2 = \frac{3}{4}(u^2 + v^2) + \frac{1}{2}w^2. \quad (19)$$

The temperature correction is now simply

$$T_0 = T_r + \frac{1}{403} \left(\frac{3}{4}(u_0^2 + v_0^2) + \frac{1}{2}w_0^2 \right), \quad (20)$$

where we again let the subscripts denote corrected and raw values.

5.4 Statistics

Averages of 10min and 30min has been constructed. Both ensembles are represented in three different coordinate systems (all right handed):

- **nesw:** Regular East (\bar{u} in the x-direction) - North (\bar{v} in the y-direction) coordinate system. The wind direction (where the wind comes from!) is defined with 0° true north and increasing clockwise, i.e. 270° denotes westerlies.
- **windvec2d:** The right-handed coordinate system is rotated around the vertical axis, such that $\bar{v} = 0$.
- **windvec3d:** First the coordinate system is rotated as in **windvec2d**. Then it is rotated around a horizontal axis such that $\bar{v} = \bar{w} = 0$ (and still $\bar{v} = 0$).

The sonics sampling rate is 20hz. A 10min average thus contains 12.000 samples. Errors in sampling due to very fast fluctuations, data streaming or online data storage may induce interruptions in the recording. In the present statistics an average of 60 "bad" samplings within 10 minutes is allowed. The exact number of "bad" samplings allowed (as long as it is low) does, however, not influence the 10 min averages in any significant way.

In reality each sonic return a status value of 1,2,3 or 4. 1 is ok while the other three correspond to the different errors which can occur. Taking the average over the status values in 10 minutes we only include those periods in which the average is below 1.01 corresponding to on average 60 "bad" samplings.

5.4.1 10min statistic aligned with the nesw coordinatesystem

The sonic coordinate system has the x-direction towards the mast and the y-direction at 90 degrees to the right. With the z-direction pointing upwards for positive values the coordinate system is left handed. Let \mathbf{u}_i denotes the i 'th sample of the velocity vector $\mathbf{u} = (u, v, w)$ as recorded by a sonic. Statistical moments of order p of a single component j in the **nesw** coordinate system is then given by

$$\langle u_j^p \rangle_{10min} = \frac{1}{N} \sum_{i=0}^N (\mathbf{A}(\theta) \mathbf{u}_i^p)_j, \quad (21)$$

where N is the number of samples within 10 minutes. $\mathbf{A}(\theta)$ is the rotation matrix for boom direction, θ . θ is increasing clockwise with zero pointing towards north. Table 17 includes the boom directions for the different masts. $\mathbf{A}(\theta)$ is given by

$$\mathbf{A}(\theta) = \begin{pmatrix} -\sin \theta & -\cos \theta & 0 \\ -\cos \theta & \sin \theta & 0 \\ 0 & 0 & 1 \end{pmatrix} \quad (22)$$

Mean, variance and covariance is easily obtained as

$$\bar{u}_j = \langle u_j \rangle \quad (23)$$

$$covar(u_i u_j) = \langle u_i u_j \rangle - \langle u_i \rangle \langle u_j \rangle \quad (24)$$

Table 17. Boom directions for the different masts.

mast id	M0	M1	M2	M3	M4	M5	M6	M7	M8	M9
boom direction	151°	179°	179°	175°	180°	175°	179°	180°	180°	178°

5.4.2 Statistics aligned with the mean wind vector

The 10 minute data in the **nesw** coordinate system is the foundation of all other statistics. In **windvec2d** and **windvec3d** the mean velocity is in the x-direction, \bar{u} is orientated along the horizontal and 3-dimensional mean wind vector respectively, so that $\bar{v} = 0$. In **windvec2d** \bar{w} is positive upwards. The two representations are obtained by performing the following rotations

$$\bar{u}_i^R = R_{ij} \langle u_j \rangle \quad (25)$$

$$\text{covar}(u_i u_j)^R = R_{ik} \langle u'_k u'_l \rangle R_{jl}, \quad (26)$$

with $u'_k = u_k - \langle u_k \rangle$. In the **windvec2d** case the rotation matrix $\mathbf{R} = (\mathbf{r}_1, \mathbf{r}_2, \mathbf{r}_3)$ is given by

$$\mathbf{r}_1 = (\bar{u}, \bar{v}, 0) / \sqrt{\bar{u}^2 + \bar{v}^2} \quad (27)$$

$$\mathbf{r}_3 = (0, 0, 1) \quad (28)$$

$$\mathbf{r}_2 = \mathbf{r}_3 \times \mathbf{r}_1 / |\mathbf{r}_3 \times \mathbf{r}_1|, \quad (29)$$

While it in the **windvec3d** case is given by

$$\mathbf{r}_1 = (\bar{u}, \bar{v}, \bar{w}) / \sqrt{\bar{u}^2 + \bar{v}^2 + \bar{w}^2} \quad (30)$$

$$\mathbf{r}_{3,tmp} = (0, 0, 1) \quad (31)$$

$$\mathbf{r}_2 = \mathbf{r}_{3,tmp} \times \mathbf{r}_1 / |\mathbf{r}_{3,tmp} \times \mathbf{r}_1| \quad (32)$$

$$\mathbf{r}_3 = \mathbf{r}_1 \times \mathbf{r}_2 / |\mathbf{r}_1 \times \mathbf{r}_2|. \quad (33)$$

The 30 minutes averaged data are constructed from the 10 minutes averaged data in the **nesw** coordinate system. Three consecutive 10 minutes blocks are averaged before rotated into 30 minutes **windvec2d** and **windvec3d** ensembles.

5.4.3 Turbulence statistics over flat terrain

Mast *M0* is located on the sea west of Bolund while mast *M9* is located on the isthmus just east of Bolund. Both of them are therefore located in fairly flat terrain. We have calculated the friction velocity u_* and the Monin-Obukhov length L (actually we store the reciprocal $1/L$ in the database) for the sonics positioned at 5m (the only represented in all four periods for both mast *M0* and *M9*). Both parameters are easily accessible from the 10 minutes as well 30 minutes data in the **windvec2d** coordinate system:

$$u_* = |\overline{u'w'}|^{1/2} \quad (34)$$

$$L = -\frac{u_*^3}{\kappa(g/\theta)\overline{w'\theta'}|_{z=5m}} \quad (35)$$

A few of the averages have a very small but unfortunately negative values of $-\overline{u'w'}$ (positive momentum flux) at the sonic height at 5m. Taking the absolute value guarantee u_* to be a real number. In calculating L we make no distinction between $\overline{w'T'}$ and $w'\theta'$, the error associated with this generalization will by all means be vanishing small, the same can be said about the heat flux being recorded at 5m instead of at the surface. Figure 21 displays u_* and $1/L$ for the first measurement period for 30 minutes fluxes. There is a nice correspondence between the two masts as expected.

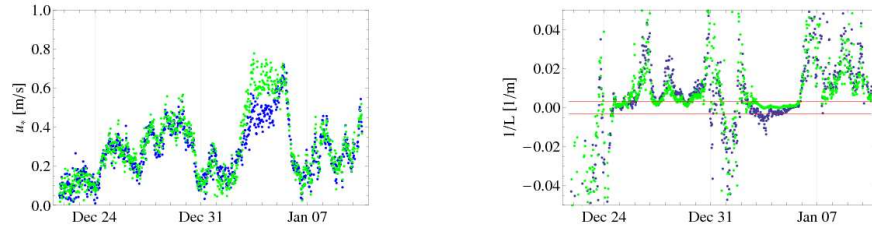


Figure 21. left u_* at mast $M0$ (blue) and $M9$ (green) right $1/L$. The horizontal lines marks the limit of neutral stability.

5.4.4 Validation of corrections

Since mast $M0$ and $M9$ are located on fairly flat terrain we can use measurements from two masts to validate the flow corrections due to flow distortion just described. In Figure 22 we show the tilt for the two masts. The left panel shows $M0$ while $M9$ is presented in the right. Generally there is, as perhaps expected, a rather high deviation from zero in both the corrected and uncorrected data for both masts in the direction of the boom (the vertical dotted lines). Also in the direction towards Bolund we can see significant deviations in both data. It, however, looks like the corrected data behaves slightly better (they are closer to zero degrees) although it is far from perfect and no general trends are observed. The data comes from a height of only 5 meters which means that small obstacles on the isthmus upwind probably blur the picture. We can probably disregard the effect from ocean waves since the data presented here are averaged over 30 minutes. We can conclude the discussion on the figures by saying that the error associated with measuring tilt is a couple of degrees.

In Figure 23 we see the one-dimensional velocity spectra $F_i(k_1)$ (see [13] for a definition). In the inertial range the slope is close to $-5/3$ and there we have a general relationship between the different $F_i(k_1)$ for isotropic turbulence, namely that $F_1(k_1) = 3/4 F_2(k_1) = 3/4 F_3(k_1)$ if $F_1(k_1)$ is in the direction of k_1 . In the figures we have therefore multiplied $F_2(k_1)$ (green) and $F_3(k_1)$ (blue) with $3/4$. Whereas curves for the three uncorrected raw spectra (dashed lines) for both mast $M0$ (left panel) and mast $M9$ (right panel) are far from collapsing (in the inertial range), the corrected ones (solid lines) do almost collapse. The corrections therefore seem to be important in order to obtain the right spectral results.

In order to verify the corrections made to the sonic temperature we compare the temperature flux $w'T'$ with the temperature difference ΔT measured by thermometers (P2642A Pt 100/500 sensors and P2029 Radiation shields) from two heights around the sonics at 5m. For mast $M0$ the thermometers are positioned at 2m and at 12m while for mast $M9$ they are positioned at 1.35m and at 15.10m. To get the potential temperature we subtract the dry adiabatic lapse rate

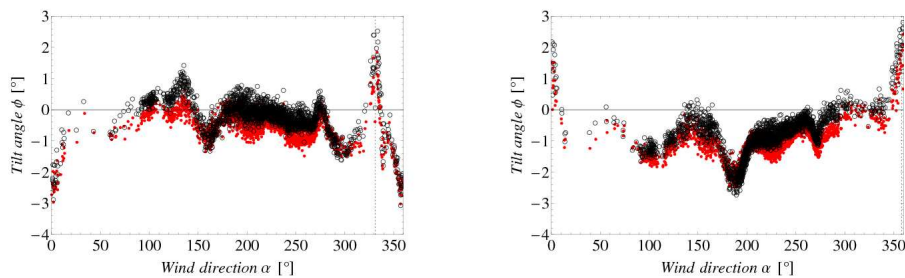


Figure 22. Tilt as a function of wind direction. left: $M0$ and right: $M9$. The vertical dotted lines indicate the boom direction. Red dots represent uncorrected values while open circles represent corrected values. Each data point represents 30 minutes of averaging.

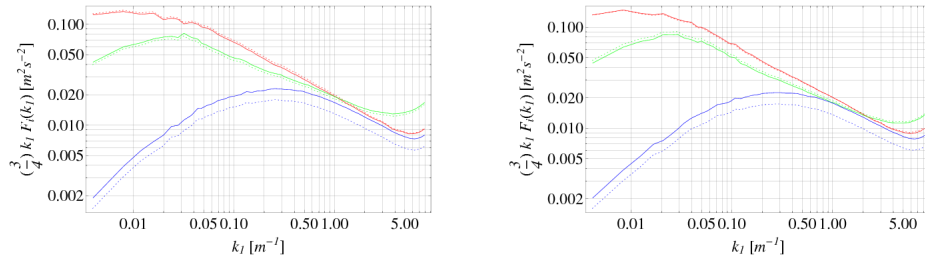


Figure 23. One-dimensional velocity spectra $F_i(k_1)$. $F_2(k_1)$ (green) and $F_3(k_1)$ (blue) have been multiplied with $3/4$. The solid lines are from the corrected velocities while dashed ones are from uncorrected. Left: Mast M0, right: Mast M9. Data from 200712261800 to 200712291800 has been used.

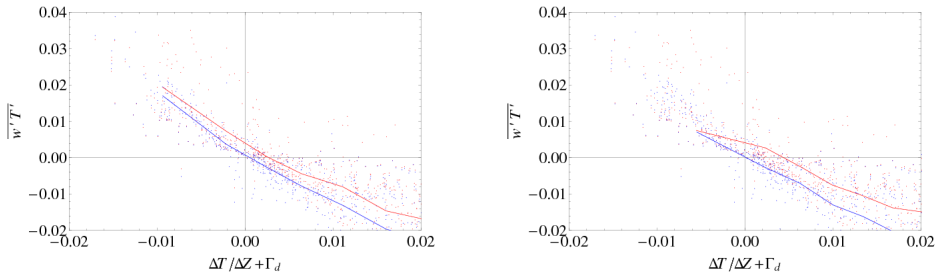


Figure 24. Temperature flux $\overline{w'T'}$ as a function of dry adiabatic temperature difference $\Delta T / \Delta z + \Gamma_d$. Left: Mast M0, right: Mast M9. Blue color represent corrected values while red represent uncorrected values. The flux is averaged over 30min.

$\Gamma_d = -0.0098\text{K/m}$. The results are shown in Figure 24. Again the left panel show mast M0 while M9 is presented in the right panel. In both cases (best for mast M9) the correction (blue curves) surely helps and the flux equals zero for a zero temperature difference as expected. The overall behavior is close to linear in agreement with a flux-gradient hypothesis with constant turbulent exchange coefficient.

Like the temperature flux we have also looked at the temperature variance $\overline{T'T'}$ as a function of $\Delta T / \Delta z + \Gamma_d$. We expect the variance to be zero at zero temperature difference and symmetric else where. The results are shown in Figure 25. The results are far from convincing and no improvement is observed. There is a clear offset in the first quadrant. Many factors might influence this result. First of all the variance measured by the sonics might not be representative for the whole layer between the two temperature sensors. Also the atmosphere is not in neutral condition conditions all the time.

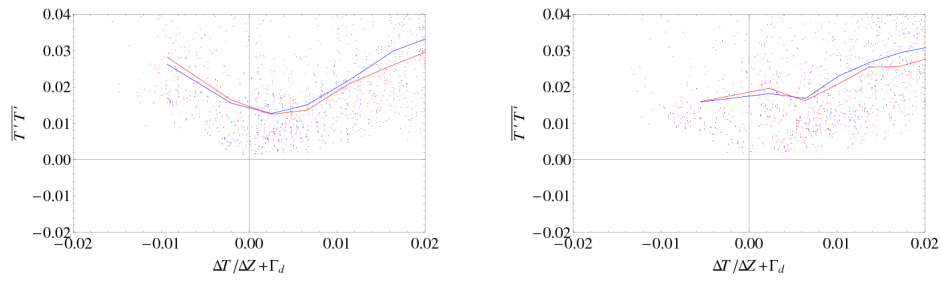


Figure 25. Temperature variance $\overline{T'T'}$ as a function of dry adiabatic temperature difference $\Delta T / \Delta z + \Gamma_d$. Left: Mast M0, right: Mast M9. Blue color represent corrected values while red represent uncorrected values. The variance is taken as 30min averages.

6 MySQL database

6.1 Overview

All measurements taken during the Bolund campaign is stored in a MySQL database that is briefly described in this chapter. The tables and columns of the database are not described in detail, instead three examples on how to retrieve data are given. Additionally, Chapter 4 (particularly Table 5-14) gives the instrument ID used in the database. In order to gain access to the Bolund database please contact Risø DTU (access will not be granted before year-end 2009).

6.2 Tables in MySql

A brief overview of the different tables in the Bolund MySQL database containing data.

- **caldata_x_1hz**: Temperature sensor data recorded at 1 hz. x runs from 1 to 4 and denotes measurement period (see Table 15 in Chapter 5).
- **caldata_x_5hz**: Cup anemometer data recorded at 5 hz. x runs from 1 to 4 and denotes measurement period (see Table 15 in Chapter 5).
- **caldata_x_20hz**: Sonic data recorded at 20 hz. x runs from 1 to 4 and denotes measurement period (see Table 15 in Chapter 5).
- **metek3dcorr_x_20hz**: Metek 3D corrected sonic data recorded at 20 hz. x runs from 1 to 4 and denotes measurement period (see Table 15 in Chapter 5).
- **calmeans** Data from all sensors (temperature, cups and sonics): 10 min averages.
- **calmin** Data from all sensors (temperature, cups and sonics): 10 min minimum.
- **calmax** Data from all sensors (temperature, cups and sonics): 10 min maximum.
- **calstd** Data from all sensors (temperature, cups and sonics): 10 min standard deviation.
- **stat_nesw_10min** Sonic data (not 3D corrected): 10 min data. Coordinate system: north-east-south-west.
- **stat_nesw_30min** Sonic data (not 3D corrected): 30 min data. Coordinate system: north-east-south-west.
- **stat_stability_10min** Sonic data (not 3D corrected): 10 min data. u_* and $1/L$ for Mast 0 and Mast 9 (def. of u_* see Section 5.4). Coordinate system: north-east-south-west.
- **stat_stability_30min** Sonic data (not 3D corrected): 30 min data. u_* and $1/L$ for Mast 0 and Mast 9 (def. of u_* see Section 5.4). Coordinate system:north-east-south-west.
- **stat_windvector2d_10min** Sonic data: 10 min data. Coordinate system: in horizontal wind direction.
- **stat_windvector2d_30min** Sonic data: 30 min data. Coordinate system: in horizontal wind direction.
- **stat_windvector3d_10min** Sonic data: 10 min data. Coordinate system: in 3D wind direction.
- **stat_windvector3d_30min** Sonic data: 30 min data. Coordinate system: in 3D wind direction.
- **stat_nesw_metek3dcorr_10min** Sonic data: 10 min data. Coordinate system: north-east-south-west. Metek 3D corrected.

- **stat_nesw_metek3dcorr_30min** Sonic data: 30 min data. Coordinate system: north-east-south-west. Metek 3D corrected.
- **stat_stability_metek3dcorr_10min** Sonic data: 10 min data. u_x and $1/L$ for Mast 0 and Mast 9 (def. of u_x see Section 5.4). Coordinate system: north-east-south-west. Metek 3D corrected.
- **stat_stability_metek3dcorr_30min** Sonic data: 30 min data. u_x and $1/L$ for Mast 0 and Mast 9 (def. of u_x see Section 5.4). Coordinate system: north-east-south-west. Metek 3D corrected.
- **stat_windvector2d_metek3dcorr_10min** Sonic data: 10 min data. Coordinate system: in horizontal wind direction. Metek 3D corrected.
- **stat_windvector2d_metek3dcorr_30min** Sonic data: 30 min data. Coordinate system: in horizontal wind direction. Metek 3D corrected.
- **stat_windvector3d_metek3dcorr_10min** Sonic data: 10 min data. Coordinate system: in 3D wind direction. Metek 3D corrected.
- **stat_windvector3d_metek3dcorr_30min** Sonic data: 30 min data. Coordinate system: in 3D wind direction. Metek 3D corrected.
- **platformheight**: The distance between water level and platform base at M0 (set to 30 cm for the official map, see Section 4.2)
- **zephir_site2_unit102_x** Five tables (x = spectra, spectradef, spectraf lelog, stream10min, stream3sec) containing Doppler spectra sampled 50 times per second and derived three second and ten minute average wind vectors. These are measured 8.5 meters south of mast 2 by the lidar ZephIR unit 102.
- **zephir_site3_unit102_x** Same as above, but the instrument has been moved to 10 meters south of mast 3.
- **zephir_site9_unit2_x** Again five tables as above, but now from the lidar instrument ZephIR unit 2 adjacent to mast 9.
- **zephir_site3_unit102_x** Standard output, which does not include Doppler spectra, from ZephIR unit 102. Data from the two positions close to mast 2 and 3 are all in the same table. These three tables essentially duplicate zephir_x_unit102_stream10min and zephir_x_unit102_stream3sec.

6.3 Example 1: Retrieving sonic data

Lets say you want to get the horizontal velocity (10min average and Metek corrected), the tilt and the wind direction recorded at sonic *M1_S_9* in those conditions where the wind direction recorded at sonic *M0_S_5* is true west. If we set the margin on wind direction to ± 5 degrees the following statement executed in MySQL will give the desired result:

```
SELECT
m.sonic_id,
m.name,
m.u_mean,
m.tilt,
m.windDir
FROM
bolund.stat_windvec2d_metek3dcorr_10min m,
```

```

bolund.stat.windvec2d_metek3dcorr_10min m2
WHERE
m2.name=m.name and m.sonic_id="M1_S_9" AND
m2.sonic_id="M0_S_5" AND m2.windDir>265 AND m2.windDir<275

```

6.4 Example 2: Retrieving cup data

Another example illustrates the retrieval of both sonic and cup data. Lets say that we want to calculate the roughness length at Mast M9, assuming a logarithmic profile in neutral conditions. In order to justify the latter we choose situations with wind speed exceeding 10 m/s and stability $|1/L| < 0.002$. Since the flow is distorted by the hill in westerly directions we choose only to look at situations where the wind is from the east. Again we use the 10min average and Metek corrected sonic data. Since we only have a sonic placed in 5 m we also use the cup data in 1.9, 5, 9 and 15.6 m. We set the margin on wind direction to ± 10 degrees. In MySQL the executing command should look like:

```

SELECT
m.ustar,
m1.u_mean,
m2.M9_Cup_2,
m2.M9_Cup_5,
m2.M9_Cup_9,
m2.M9_Cup_15
FROM
bolund.stat.stability_metek3dcorr_10min m,
bolund.stat.windvec2d_metek3dcorr_10min m1,
bolund.calmeans m2
WHERE
m2.name=m1.name AND
m1.name=m.name AND
m.sonic_id="M9_S_5" AND
m1.sonic_id="M9_S_5" AND
m1.u_mean>10 AND
ABS(m.invL<0.002) AND
m1.windDir>80 AND m1.windDir<100

```

We can then construct the average $\langle u/u_* \rangle$ and plot the data as a function of $\log(z)$. The result is showed in Figure 26. From the straight line fit we can obtain the local roughness length, $z_0 = 6$ mm.

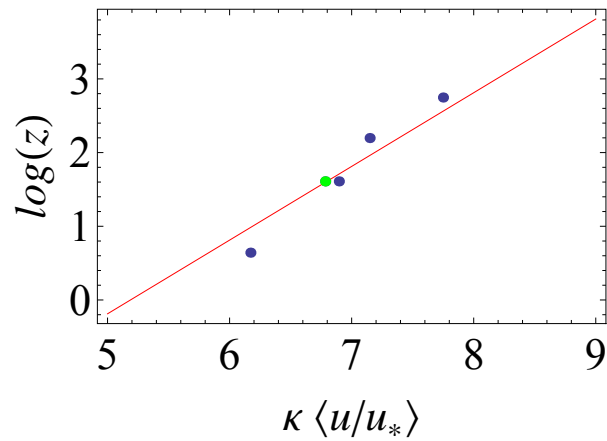


Figure 26. $\langle u/u_* \rangle$ with height. The straight line is the best linear fit with slope one.

6.5 Example 3: Retrieving lidar data

This example illustrates the retrieval of both Lidar and cup data. The wind speed measured by the lidar close to mast M9 at a height of 14 m is compared to the cup anemometer speed at 15.6 m above the ground at the same mast (see Figure 27)

Select

```
c.M9_Cup_15,
```

```
z.U
```

```
from
```

```
bolund.zephir_site9_unit2_stream10min z,
```

```
bolund.calmeans c
```

```
where z.Points_in_fit>100 AND z.turb<0.05 AND z.U is not Null AND
```

```
c.M9_Cup_15 is not NULL AND z.height=14 and z.name = c.name
```

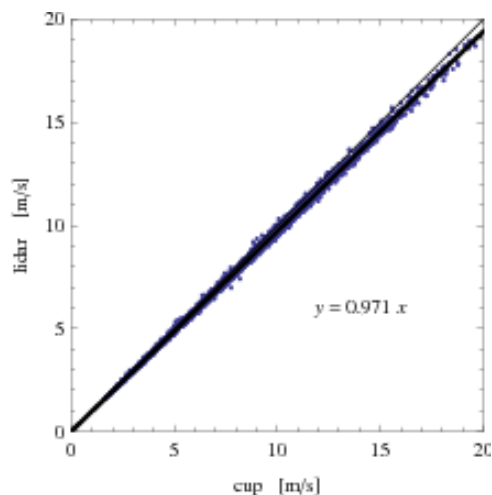


Figure 27. Comparison of the horizontal wind speed measured at mast M9 at 15 m with a cup anemometer versus a lidar.

Appendix A

Optech Airborne Laser Terrain Mapper, ALTM 3100EA

New

Introducing
the new Optech **ALTM 3100EA**

GET THE ACCURACY YOU'VE ALWAYS WANTED

The new ALTM 3100EA (Enhanced Accuracy) is the latest in a series of Optech Airborne Laser Terrain Mappers that now allows you to zero in on the fine details you may have been missing. Under optimal conditions get results as accurate as ± 3 cm, 2-sigma, (500 m, 33 kHz, scan angle at $\pm 10^\circ$). With the enhanced ability to reduce elevation noise, the 3100EA lets you detect fine target details that are required for your large scale mapping needs.

When you really need to get those critical details, the choice is clear -

choose the Optech ALTM 3100EA.

IT'S ALL ABOUT THE SCIENCE

Optech

ALTM 3100EA: 3,500 m altitude! 100,000 laser pulses per second!

ALTM 3100EA Specifications

Airborne Module

Operating altitude 80-3,500 m nominal
Horizontal accuracy 1/5,500 x altitude; 1-sigma

Elevation accuracy ± 1 -sigma

Laser Rep Rate (kHz)	500 m altitude	1000 m altitude	2000 m altitude	3000 m altitude
33	<5 cm	<10 cm	<15 cm	<20 cm
50	<5 cm	<10 cm	<15 cm	N/A
70	<10 cm	<10 cm	<15 cm	N/A
100	<10 cm	<10 cm	N/A	N/A

Note: Quoted accuracies do not include GPS errors.

Range capture Up to 4 range measurements for each pulse including last

Intensity capture 12 bit dynamic range for each measurement

Scan frequency Variable; maximum 70 Hz

Scan angle Variable from 0 to $\pm 25^\circ$, in increments of $\pm 1^\circ$

Scanner product Scan angle x scan frequency $\leq 1,000$

Roll compensation 5 Hz update rate
(Scan angle + Roll comp. angle = 25° , e.g., $\pm 20^\circ$ scan allows $\pm 5^\circ$ compensation)

Swath width Variable from 0 to 0.93 x altitude (m)

Position orientation system Applanix - POS/AV including internal 12 channel dual frequency 2 Hz GPS receiver

Spot distribution Sawtooth, uniform across 96% of scan

Laser repetition rate 33 kHz (max. altitude (AGL) 3.5 km)
50 kHz (max. altitude (AGL) 2.5 km)
70 kHz (max. altitude (AGL) 1.7 km)
100 kHz (max. altitude (AGL) 1.1 km)

Data storage hard drives Ruggedized removable hard drive
Minimum 7 hr. continuous log time @ 100 kHz

Beam divergence Dual divergence 0.3 mrad (1/e) or 0.8 mrad (1/e)

Laser classification Class IV (FDA 21 CFR)

Power requirements 28 VDC, 35 A (maximum)

Operating temperature Control rack: +10°C to +35°C

(air temperature) Sensor head: -10°C to +35°C
(assuming the use of sensor insulating jacket)

Storage temperature -10°C to +50°C

Humidity 0 - 95% non-condensing

Control Rack

Vibration-isolated case:
Dimensions/weight (in-flight) 65 cm x 59 cm x 49 cm/53.2 kg covers removed, with removable hard drive installed

Cables/laptop 7.6 kg/3 kg

Sensor Head

Fits standard camera mounts or mounts directly to floor

Overall dimensions/weight (in-flight) 26 cm x 19 cm x 57 cm/23.4 kg (incl. sensor insulating jacket)

Minimum opening 19.2 cm x 25.5 cm (flight direction)

Processing Software

REALM Survey Suite Differential kinematic GPS solution
Trajectory optimization from multiple base stations
XYZ point calculations module
Vegetation classification/ extraction feature
Windows NT/2000/XP compatible

GPS Ground Support

Multiple base stations Any dual frequency receiver with Rinex output

Note: to meet its stated accuracy, the ALTM must receive GPS data of sufficient quality. GPS data quality shall be viable only when all of the following conditions are met:

- At least four satellites are in lock (tracked by the receiver) throughout the survey
 - Elevation of the satellites is good (i.e., PDOP <4)
 - Aircraft stays within 30 km of the GPS base station
- If one or more of these conditions is not met, or if any source of electromagnetic interference causes the GPS receivers to repeatedly lose lock, the specified accuracy of the ALTM will be compromised.

Specifications subject to change without notice.



USA OFFICE:

Optech International, Inc.

7225 Stennis Airport Drive • Suite 400
Kiln, Mississippi 39556 USA • Tel: [228] 252-1004
Fax: [228] 252-1007 • Web: www.optechint.com
Email: inquiries@optechint.com

© Copyright 2006, Optech Incorporated. All rights reserved. 02/5986

CANADIAN OFFICE:

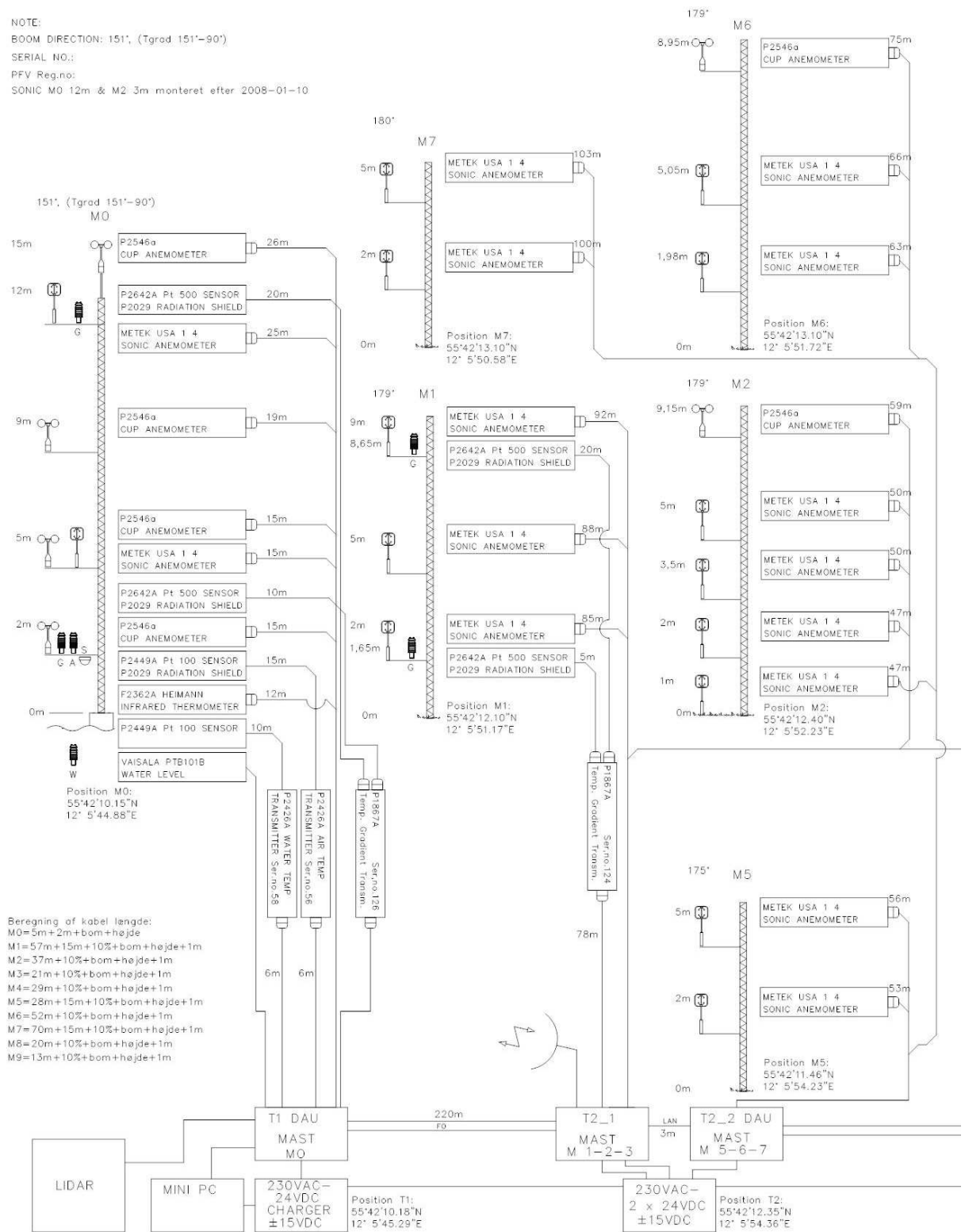
Optech Incorporated

300 Interchange Way • Vaughan, ON
Canada L4K 5Z8 • Tel: [905] 660-0808
Fax: [905] 660-0829 • Web: www.optech.ca/accuracy
Email: science@optech.ca

Appendix B

Appendix B: Diagram of Instrumentation

NOTE:
 BOOM DIRECTION: 151°, (Tgrad 151°-90°)
 SERIAL NO.:
 PFV Reg.no:
 SONIC M0 12m & M2 3m monteret efter 2008-01-10



Appendix C

In this appendix the look-up tables for sine and cosine coefficient in eqn. 17 are given. The sum runs over $i \in \{0, 3, 6, 9\}$. Since the sine term vanish for $\alpha_r = 0$ we are left with seven coefficients for each value of ϕ_r .

Table 18. Look-up table for $n_c(\alpha_r, \phi_r)$

ϕ	$C_{n_c,0}$	$C_{n_c,3}$	$C_{n_c,6}$	$C_{n_c,9}$	$S_{n_c,3}$	$S_{n_c,6}$	$S_{n_c,9}$
-50	1.23095	-0.0859199	-0.0674271	0.0160088	0.0363397	0.0141701	-0.0271955
-45	1.19323	-0.0430575	0.00309311	0.0430652	0.0225135	0.000740028	-0.0114045
-40	1.17255	-0.0206394	0.0145473	0.0399041	-0.00592748	-0.00650942	-0.00762305
-35	1.15408	-0.00768472	0.0614486	0.0382888	0.0123096	-0.0124673	-0.00598534
-30	1.12616	0.00000536	0.0636543	0.0386879	0.0153428	-0.014148	-0.000210096
-25	1.09976	0.00667086	0.0705414	0.0198549	0.0165582	-0.0114517	-0.00115495
-20	1.07518	0.00583915	0.0591098	0.011127	0.0104259	-0.00665653	0.00119842
-15	1.05173	0.00731099	0.0527018	0.00230123	0.00587927	-0.00229463	-0.00297294
-10	1.02428	0.00885121	0.0330304	-0.000597029	0.00340367	-0.000745781	-0.000283634
-5	1.011	0.00930375	0.0218448	-0.0046575	0.00203972	-0.00112652	0.00179908
0	1.00672	0.0105659	0.0034918	-0.00844128	0.00228384	-0.000824805	0.000200667
5	1.01053	0.00885115	-0.0182222	-0.00894106	-0.000719837	-0.000420398	-0.00049521
10	1.02332	0.00618183	-0.035471	-0.00455248	-0.00215202	-0.00229836	-0.000309162
15	1.04358	0.00648413	-0.0494223	0.000323015	-0.00396036	-0.00465476	-0.000117245
20	1.06928	0.00733521	-0.0638425	0.0101036	-0.00829634	-0.0073708	-0.00051887
25	1.09029	0.00396333	-0.0647836	0.0187147	-0.0126355	-0.0115659	0.000482614
30	1.11877	0.00299473	-0.0661552	0.0293485	-0.00957493	-0.00963845	0.0029231
35	1.13779	0.00812517	-0.0526322	0.0341525	-0.00971735	-0.0114763	0.0013481
40	1.16659	-0.00869651	-0.0537855	0.0290825	-0.0000989207	-0.0133731	0.0117738
45	1.18695	-0.0289647	-0.0461693	0.030231	-0.0121524	-0.00667729	0.00565286

Table 19. Look-up table for $\alpha_c(\alpha_r, \phi_r)$

ϕ	$C_{\alpha_c,0}$	$C_{\alpha_c,3}$	$C_{\alpha_c,6}$	$C_{\alpha_c,9}$	$S_{\alpha_c,3}$	$S_{\alpha_c,6}$	$S_{\alpha_c,9}$
-50	-10.7681	1.83694	8.12521	1.76476	-0.120656	-0.31818	1.30896
-45	-7.57048	2.25939	4.22328	-0.0394204	-0.112215	-0.289935	1.99387
-40	-6.77725	0.293479	3.05333	-1.16341	0.433886	0.207458	1.05195
-35	-4.12528	2.24741	0.286582	-0.936084	0.205636	-0.399336	1.57736
-30	-2.00728	3.63124	-0.325198	-0.821254	0.236536	-0.303478	0.854497
-25	-3.1161	3.91749	-0.682098	-0.274558	0.401386	-0.531782	0.470723
-20	-1.73949	3.5685	-0.253107	0.0306742	0.236975	-0.290767	-0.224723
-15	-2.59966	2.7604	-0.425346	0.0557135	0.0392047	0.222439	-0.364683
-10	-1.80055	2.02108	-0.259729	0.161799	0.117651	0.513197	-0.0546757
-5	-1.02146	1.22626	-0.469781	-0.177656	0.402977	0.408776	0.513465
0	0.152354	0.208574	0.051986	-0.102825	0.480597	-0.0710578	0.354821
5	0.310938	-0.703761	-0.0131663	0.0877815	0.546872	-0.342846	0.176681
10	0.530836	-1.68132	-0.0487515	0.0553666	0.524018	-0.426562	-0.0908979
15	1.70881	-2.46858	-0.487399	0.207364	0.638065	-0.458377	-0.230826
20	2.38137	-3.37747	0.026278	0.0749961	0.759096	0.105791	0.0287425
25	3.81688	-4.13918	-0.690113	0.170455	0.474636	0.424845	0.232194
30	3.49414	-3.82687	-0.229292	0.54375	0.322097	0.387805	0.823967
35	4.1365	-3.22485	0.752425	0.755442	0.623119	0.250988	1.26713
40	5.04661	-2.53708	1.23398	0.623328	0.653175	-0.359131	1.43131
45	4.26165	-3.12817	2.61556	0.0450348	-0.330568	-0.34354	0.81789

Table 20. Look-up table for $\phi_c(\alpha_r, \phi_r)$

ϕ	$C_{\phi_c,0}$	$C_{\phi_c,3}$	$C_{\phi_c,6}$	$C_{\phi_c,9}$	$S_{\phi_c,3}$	$S_{\phi_c,6}$	$S_{\phi_c,9}$
-50	5.77441	-2.19044	0.123475	-0.229181	0.226335	0.271943	0.0434668
-45	3.82023	-1.6847	0.315654	0.562738	0.175507	-0.0552129	-0.110839
-40	2.29783	-1.04802	0.0261005	0.239236	0.125053	-0.310631	0.388716
-35	1.37922	-1.0435	0.302416	-0.0112228	0.333846	-0.459678	0.172019
-30	0.837231	-0.593247	-0.199916	-0.0591118	0.19883	-0.307377	0.182622
-25	-0.0588021	-0.0720115	-0.6826	-0.253726	0.348259	-0.322761	0.0059973
-20	-0.0333721	0.101664	-1.41617	-0.136743	0.332169	-0.244186	-0.0612597
-15	0.0423739	0.0428399	-1.90137	-0.187419	0.148025	0.06782	-0.0317571
-10	0.318212	0.126425	-2.07763	-0.0341571	0.198621	0.178598	0.103543
-5	0.721731	-0.0274247	-2.10221	-0.081822	0.36773	0.0848013	0.184226
0	1.65254	-0.0582368	-2.18993	-0.0802346	0.234886	-0.0545883	-0.0092531
5	2.49129	-0.116475	-2.11283	0.112364	0.247405	-0.115218	-0.0682998
10	2.99839	-0.0867988	-2.04382	0.219581	0.207231	-0.0981521	-0.0581594
15	3.55129	-0.160112	-1.8474	0.22217	0.2794	-0.0323565	-0.0951596
20	3.20977	-0.137282	-0.966014	0.183032	0.380154	0.155093	-0.0557369
25	3.38556	-0.0596863	-0.898053	0.20526	0.39357	0.421141	-0.00842409
30	3.18846	0.266264	-0.0951907	0.166895	0.373018	0.338146	0.187917
35	2.60134	0.442007	0.211612	-0.114323	0.359926	0.224424	0.209482
40	2.04655	1.08915	0.470385	-0.333096	0.268349	0.263547	0.264963
45	0.987659	1.54127	0.815214	-0.504021	-0.0835985	0.197387	0.0819912

References

- [1] A. Bechmann, J. Johansen, and N. Sørensen. The bolund experiment - design of measurement campaign using cfd. Technical Report Risø-R-1623(EN), Risø National Lab., Roskilde, Denmark, 2007.
- [2] P.S. Jackson and J.C.R. Hunt. Turbulent wind flow over a low hill. *Quart. J. R. Met. Soc.*, 101:929:955, 1975.
- [3] P.A. Taylor and H.W. Teunissen. Askervein '82: Report on the september/october 1982 experiment to study boundary-layer flow over askervein, south uist. *Atmos. Environ. Service, Downsview, Ontario*, Technical Report MSRB-83-8, 1983.
- [4] P.A. Taylor and H.W. Teunissen. The askervein hill project: Report on the sept./oct. 1983, main field experiment. *Atmos. Environ. Service, Downsview, Ontario*, Technical Report MSRB-84-6, 1984.
- [5] H. Charnock. Wind stress over a water surface. *Quart J Roy Meteorol Soc*, 81:639–640, 1955.
- [6] N.O. Jensen, E.L. Petersen, and I. Troen. Extrapolation of mean wind statistics with special regard to wind energy applications. *WCP-86. World meteorological Organization, 1984. WMO/TD-No.15*, 1984.
- [7] IEC 61400-12-1. Wind turbines - part 12-1: Power performance measurements of electricity producing wind turbines. 2005.
- [8] MEASNET (<http://www.measnet.com>). Cup anemometer calibration procedure version 1 september 1997. 1997.
- [9] D. A. Smith, M. Harris, A. S. Coffey, T. Mikkelsen, H. E. Jrgensen, J. Mann, N.O. Danielian, R.Jensen, E.L. Petersen, and I. Troen. Wind lidar evaluation at the danish wind test site hvsre. *Wind Energy*, 9(1-2):87–93, 2006.
- [10] Ferhat Bingl, Jakob Mann, and Dimitri Foussekis. Modeling conically scanning lidar error in complex terrain with WAsP Engineering. *Meteorol. Z.*, 18(2):189–195, 2009.
- [11] Flow distortion correction for 3-d flows as measured by METEK's ultrasonic anemometer USA-1. *Metek GmbH*, 3. March 2004.
- [12] H. Liu, G. Peters, and T. Foken. *Boundary-Layer Meteorology*, 100:459–468, 2001.
- [13] S.B. Pope. *Turbulent Flows*. Cambridge Univ. Press, Cambridge, England, U.K., 2000.

Risø DTU is the National Laboratory for Sustainable Energy. Our research focuses on development of energy technologies and systems with minimal effect on climate, and contributes to innovation, education and policy. Risø DTU has large experimental facilities and interdisciplinary research environments, and includes the national centre for nuclear technologies.

Risø DTU
National Laboratory for Sustainable Energy
Technical University of Denmark

Frederiksborgvej 399
PO Box 49
DK-4000 Roskilde
Denmark
Phone +45 4677 4677
Fax +45 4677 5688

www.risoe.dtu.dk